5-1-2013

Assessment of Reservoir Quality and Potential Impact of Sequestered Carbon Dioxide in Diverse Lithological Reservoir Units, South Central, Mississippi, USA

Assonman D. Degny

Assessment of reservoir quality and potential impact of sequestered carbon dioxide in diverse lithological reservoir units, south central, Mississippi, USA

By

Assonman D Degny

A Thesis
Submitted to the Faculty of
Mississippi State University
in Partial Fulfillment of the Requirements
for the Degree of Master of Science
in Geosciences
in the Department of Geosciences

Mississippi State, Mississippi

May 2013

Assessment of reservoir quality and potential impact of sequestered carbon dioxide in diverse lithological reservoir units, south central, Mississippi, USA

By

Assonman D Degny

Approved:

Brenda L. Kirkland Associate Professor of Geosciences (Committee Chair)	Karen S. McNeal Associate Professor of Geosciences (Committee member)
Darrel W. Schmitz Professor of Geosciences (Committee member)	Michael E. Brown Associate Professor of Geosciences (Graduate Coordinator)
R. Gregory Dunaway Professor and Interim Dean College of Arts & Sciences	

Name: Assonman D Degny

Date of Degree: May 11, 2013

Institution: Mississippi State University

Major Field: Geosciences

Major Professor: Dr. Brenda L. Kirkland

Title of Study: Assessment of reservoir quality and potential impact of sequestered carbon dioxide in diverse lithological reservoir units, south central, Mississippi, USA

Pages in Study: 86

Candidate for Degree of Degree

This study was designed to understand the possible impact of carbon dioxide on different reservoir rocks in south-central Mississippi. Eight samples, including six from the Heidelberg field (Mississippi), were exposed to carbon dioxide under simulated subsurface conditions of elevated temperature and pressure and then analyzed using thin section petrography, scanning electron microscopy, X-ray diffraction, and focused ion beam-SEM. Three of the eight samples showed dissolution in calcite and corrosion in smectite. SEM and EDS analysis of treated sample 5 (Se-5/shaly-sandtsone) and sample 8 (S-8/dolomitic-limestone) revealed newly precipitated lath- and fibrous-like crystals composed of sulfur (S), oxygen (O), and calcium (Ca), thus interpreted as gypsum. Three-dimensional analysis using FIB of dolomitic limestone samples (Smackover Formation) revealed that gypsum crystals fill fracture porosity. This study significantly contributes to the understanding of carbon dioxide impact on reservoir rock and promotes better management of natural gas resources.

DEDICATION

This work is dedicated to my lovely family that supported me through every moment in this journey. I would have never made it this far without them. Thank you to my father, Gnamia J Degny. To my mother, Outtara Fatouma. And to my siblings, Audrey, Ezechiel, and Linda.

ACKNOWLEDGEMENTS

I would love to thank the Department of Geosciences formerly headed by Dr Darrel Schmitz and now headed by Dr Bill Cooke for giving me the opportunity to gain more knowledge in geosciences. I would love to thank every faculty and staff in the department in contributing in one way or another to making my journey at Mississippi State University pleasant and full of joys.

I especially want to thank Dr Brenda Kirkland, my advisor, mentor, and confidant. Thank you for giving me this opportunity to better myself. I will never be able to repay you for all you have done for me. You have not only taught me important concepts in geology, sedimentology, but also life lessons that will help through my entire carrier. Thank you!!! Thank you!! Thank you!!!

Thanks to Dr Lewis Brown for designing the core lab container that helped me run the carbon dioxide experiment.

I would like to also say thank you to Amanda Lawrence, Bill Monroe, I Wei-research associates at the Mississippi State University Institute for Imaging and Analytical Techniques (I^2AT) for their time, patience, expertise, and all the help provided in examining my rocks.

I would like to thank Dr. J. Yan and Dr. Adam Hall at the Joint School of Nanoscience and Nanoengineering in Greensboro, North Carolina for providing me with

the Focused Ion Beam-SEM image data and Dr's. Pal Pedersen, Dr. Kirk Czymmek (Carl Zeiss Microscopy) for the 3D reconstruction of the microstructure.

Finally, I would like to thank all graduate students in the Department of Geosciences, and all my soccer friends. I have made it through because you guys were there to listen to me when I needed it.

TABLE OF CONTENTS

LIST OF TABLES

LIST OF FIGURES

CHAPTER I

INTRODUCTION

1.1 Introduction

The objectives of this study are to assess the quality of reservoir lithologies in the Heidelberg field as a potential reservoir for carbon dioxide storage, while also determining the impact of carbon dioxide on the mineralogy, porosity, permeability, and existing fractures. The choice of the Heidelberg field, for this study, reposes solely on the fact that it represents one of the biggest and most productive reservoirs in south central Mississippi. Also, the availability of core samples and data due to intensive studies by oil companies play a major role in our choice.

Fossil fuels (e.g coal, oil, and natural gas) supply approximately 85% of the world's energy needs (Kaldi *et al*., 2009). The low cost and relative abundance of fossil fuels suggest that fossil fuels will continue to be a significant component of the energy economy for a long period of time, estimated to be around 25 to 50 years (Kaldi *et al*., 2009). The main concern, however, is that the burning of fossil fuels constitute one of the major sources of carbon dioxide, which is considered as the main greenhouse gas released to the atmosphere (Intergovernmental Panel on Climate Change [IPCC], 2005).

The capture of carbon dioxide and storage, in a geological formation, appears to be a means to reduce the emission of carbon dioxide in the atmosphere. Carbon sequestration and storage can contribute to the reduction of atmospheric and

anthropogenic carbon dioxide (Kaldi, 2009). A technical report from the IPCC has indicated the potential of at least around 2000 billion metric tons of carbon dioxide storage in geological formations (table 1) (IPCC, 2005).

Table 1.1 Storage Capacity of different geological storage options in Giga-tons (IPCC, 2005)

Reservoir Type	Lower estimate of Storage capacity (Gt carbon dioxide)	Upper estimate of Storage capacity (Gt carbon dioxide)
Oil and gas fields	675	900
Unmineable coal seams in Enhanced Coalbed Methane recovery (ECBM)	3-15	200
Deep saline formations	1000	Uncertain but possibly 10,000

As stated above, the objectives of this research are to assess the quality of reservoir lithologies in the Heidelberg field as a potential reservoir for carbon dioxide storage, while also determining the impact of carbon dioxide on the mineralogy, porosity, permeability, and existing fractures. A study of different lithologies using core samples from the Eutaw, Tuscaloosa, "Rodessa", Salem (control), and Smackover formations was conducted to characterize permeability, porosity, mineralogy, and fractures. The hypotheses to be tested are: 1) carbon dioxide, used as either a tertiary recovery tool or in carbon sequestration, will enhance the porosity, permeability, or induce a change in

mineralogy, and fractures in some rocks and 2) the effects of carbon dioxide will be different in different lithologies.

In this study, standard research petrography was used to describe core samples and thin sections. X-ray diffraction (XRD) was utilized to identify the mineralogy before and after samples were impregnated with carbonic acid (H_2CO_3). SEM-EDS was used to identify, confirm, and document the microstructure of cements, porosity, minerals, and fracture systems present. Focused Ion Beam (FIB-SEM) was used to determine the pore system and connectivity, understand the microstructure, and construct a 3D model of sample 8.

As future carbon sequestration efforts, this project is significant in that the results can be applied to secondary and tertiary oil recovery efforts, as well as the impacts of carbon dioxide storage on reservoir rocks. Carbon dioxide storage requires specific geological characteristics. The study will also suggest desireable lithologic characteristics of possible sites and provide fundamental information in preparation for carbon dioxide sequestration that can be used in secondary and tertiary oil recovery efforts. Finally, understanding the potential hazards of permanent carbon dioxide sequestration is important to protect communities near sequestration sites. Carbon dioxide can be dangerous due to leakage or migration within the subsurface and/or the surface after storage. Leakage of carbon dioxide can occur through abandonned wells or geologic features such as faults and fractures (Kaldi *et al.*, 2009). Those carbon dioxide leaks can possibily be harmfull to the environments, especially, human via water contamination. Furthermore, Carbon dioxide is classififed as the main green house gas released to the atmosphere (IPCC, 2005), preventing or reducing the emission of carbon dioxide is

imperative to protect our environment. Carbon dioxide capture and storage (CCS) in geologic reservoirs could also help mitigate its impact on the atmosphere.

1.2 Literature review

The Heidelberg field is located in the southeastern portion of Jasper County, Mississippi, near the small town of Heidelberg (fig 1). The Heidelberg is located in Twp.1 N., Rges. 12 E. and 13 E., and Twp. 10 N., Rges. 10 W. and 11 W (McCullough, 1944).

Figure 1.1 Map of Mississippi showing the area of interest, Heidelberg (area within box).

Morse (1944).

1.3 Geologic setting

The geologic history of the Heidelberg field has been linked to the Mississippi Interior Salt Basin, which one is linked to the origin of the Gulf of Mexico (Wood and Walper, 1974). The Gulf of Mexico is described as a divergent margin basin distinguished by extensional tectonics and wrench faulting (Pilger, 1981; Miller, 1982; Klitgord *et al*., 1984; Van Siclen, 1984; Pindel, 1985; Salvador, 1987; Winker and

Buffler, 1988; Mancini *et al*., 1999). During the Late Triassic, a series of tectonic events lead to the break up of the supertcontinent Pangea. This series of tectonic events continued through the the Late Jurassic with rifting and movement of the Yucatan block. The Yucatan was rimmed to the southern margin of the United States during the early Triassic (Salvador, 1991). Although early rifting may have been north-south, the general direction of rifting was detemined to be northwest-southeast (Pilger, 1981; McRae and Watkins, 1996); defining the gulf as an opening by right lateral translation (Van Siclen, 1984; Buffler and Sawyer, 1985). The overall structure and framework of the region was set up during the Triassic and Jurassic, including the Mississippi Interior Salt Basin (Salvador, 1987). Thus, the Mississippi Interior Salt Basin was classified as the interior fracture portion of a margin sag basin (Kingston *et al.*, 1983; Mancini *et al.*, 2001).

1.4 Structure and trap

The Heidelberg field is part of the Mississippi Interior Salt Basin, which is considered one of the three major petroleum plays in the Northeastern Gulf of Mexico (Bennett *et al.*, 2000). The United State Geological Society (USGS) ranked the Mississippi Interior Salt Basin one of the more important regions in North America for oil and gas accumulations (Klett *et al*., 1997; Ahlbrandt, 1999; Bennett *et al*., 2000). Production in the local reservoirs of this basin is approximatley 1.5 billion barrels of oil and 6.7 TCF of gas (Bennett *et al*., 2000). The prolific nature of the Heidelberg field is partially associated with the local structure and stratigraphy. The formation of the Mississippi Interior Salt Basin is associated with extensional rift tectonics (Martin, 1978). An addition to extensional rifting, halokinesis, which is the mobilization and flow of subsurface salt and the subsequent emplacement and resulting structure of salt bodies,

also played a role in the formation of the basin and regional structures (Mancini *et al*., 2001). The petroleum traps of the Mississippi Interior Salt Basin are directly associated with the progression and flow of the salt and related features including: 1) peripheral ridges 2) low-relief salt pillows 3) salt anticlines and turtles and 4) piercement domes (Hughes, 1968; Montgomery and Ericksen, 1997).

In earlier studies, the Heidelberg field structure was described as an up-thrust over a deep intrusive salt dome (McCullough, 1944), which can be interpreted as a graben. The graben is comprised of series of blocks due to parallel faults running through it, consequently, creating a step down in increments of 100 ft, with a maximum drop at the center, located approximately 500 ft above the Eutaw Formation (McCullough, 1944). The two major faults forming the graben are located on either side of the dome (east-west) running north-south, three-quarters of a mile apart. Between the two major faults, exist a series of diagonal cross faults, associated with intensive frictional forces in the area. The diagonal cross faults seem to be responsible for tilting, resulting in blocks being higher in the southern section than in the northern section (McCullough, 1944; Mancini, 1994, 2001). The petroleum trap of the Heidelberg field was directly linked to the overall Mississippi Interior Salt Basin structure and related to progression of salt features in the area. The trap is described as a highly faulted, high-relief dome overlying a deep-seated salt dome (fig 1.2) (Mississippi Geological Society, 1957).

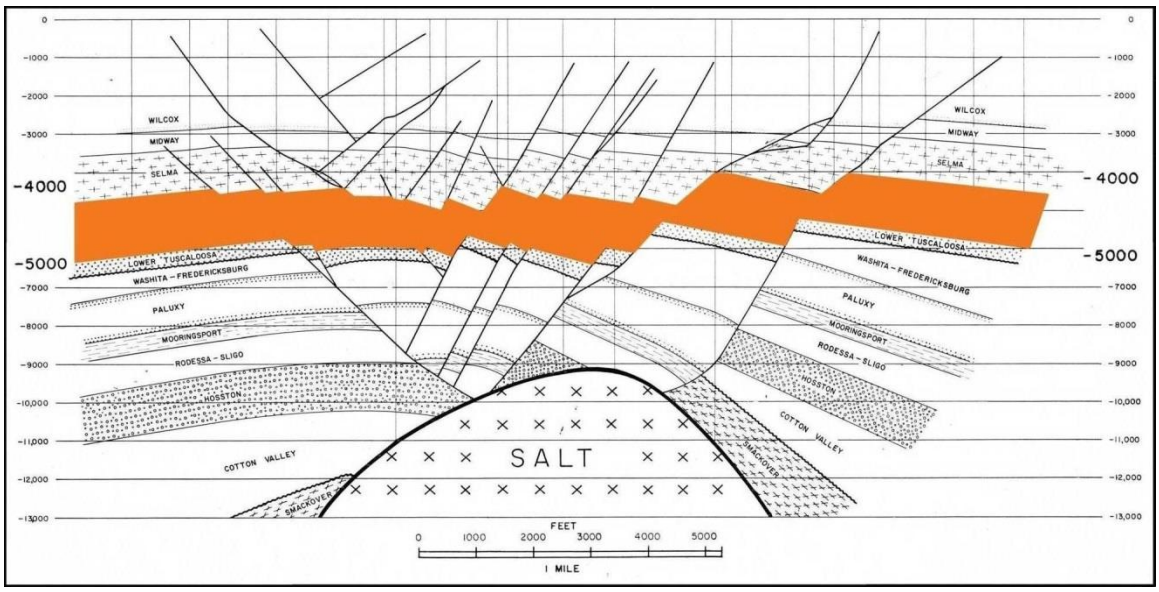

Figure 1.2 Heidelberg structure

East-west cross section of Heidelberg field illustrating depth of the Eutaw Formation in central Mississippi and salt doming as the cause for the Heidelberg Sand-Hill graben system. Producing formations highlighted (Eutaw and Tuscaloosa) Modified from Oxley and Herlihy (1974).

1.5 Stratigraphy

The Heidelberg oil field contains 12 major formations, which are shown in table 1.2. Hydrocarbon-producing units were recognized in the Heidelberg field through a series of drilling and geophysical analysis. The two main producing units are: 1) the Eutaw Formation and 2) the Tuscaloosa Formation.

The Eutaw Formation is approximately 4,518-4,916 ft (1,377.1-1,498.4 m) thick in the subsurface (Morse, 1944), and consists of 400 ft (121.9 m) of alternating sand and shale. The sands are continuous, are easily correlated throughout the area, and grade downward from shaley, calcareous, fossiliferous sands into highly porous, fine-to-medium grained, glauconitic sands (Mancini, 1994). The Eutaw Formation sediments were most likely deposited in a high energy transgressive pulse (Sohl, 1991).

Additionally, the Eutaw Formation was interpreted as having been deposited in a paralic, shallow marine environment (Mancini, 1994).

The Tuscaloosa Formation can be divided in three different units (the Upper, Marine, and Lower Tuscaloosa) with a thickness around 4,916-5,550 ft (1498 to 1691 m) (Morse, 1944, Songgiao, 1993; Mancini *et al*., 1999); and with the most abundant production in the Upper Tuscaloosa. The Upper Tuscaloosa consists of sands which are very similar in characteristic to the lower sands of the Eutaw Formation: very porous and permeable, clean, and fine to medium grained (Mississippi Geological Society, 1957). The Upper Tuscaloosa sandstones were deposited during a transgressive-regressive cycle, when the Lower Tuscaloosa sandstones were associated with major fluvial-deltaic depositional system (Sohl *et al*., 1991).

The Smackover Formation is one of the deepest formations within the Heidelberg field, approximately 12,000-13,000 ft (3657-39762 m) below the surface. The Smackover is composed of intertidal to subtidal laminated and microbial carbonate mudstone, subtidal peloidal wackestone and packestone, and subtidal to intertidal peloidal, ooid, oncoidal packestone and grainstone interbedded with laminated and fenestral carbonate mudstones (Mancini and Benson, 1980; Benson, 1988; Bearden *et al*., 2000). The Smackover was deposited on a carbonate ramp surface during the Jurassic transgression (Mancini and Benson, 1980; Benson, 1988).

Table 1.2 Stratigraphy for the eastern Gulf Coastal Plain. (Mancini *et al*., 2001).

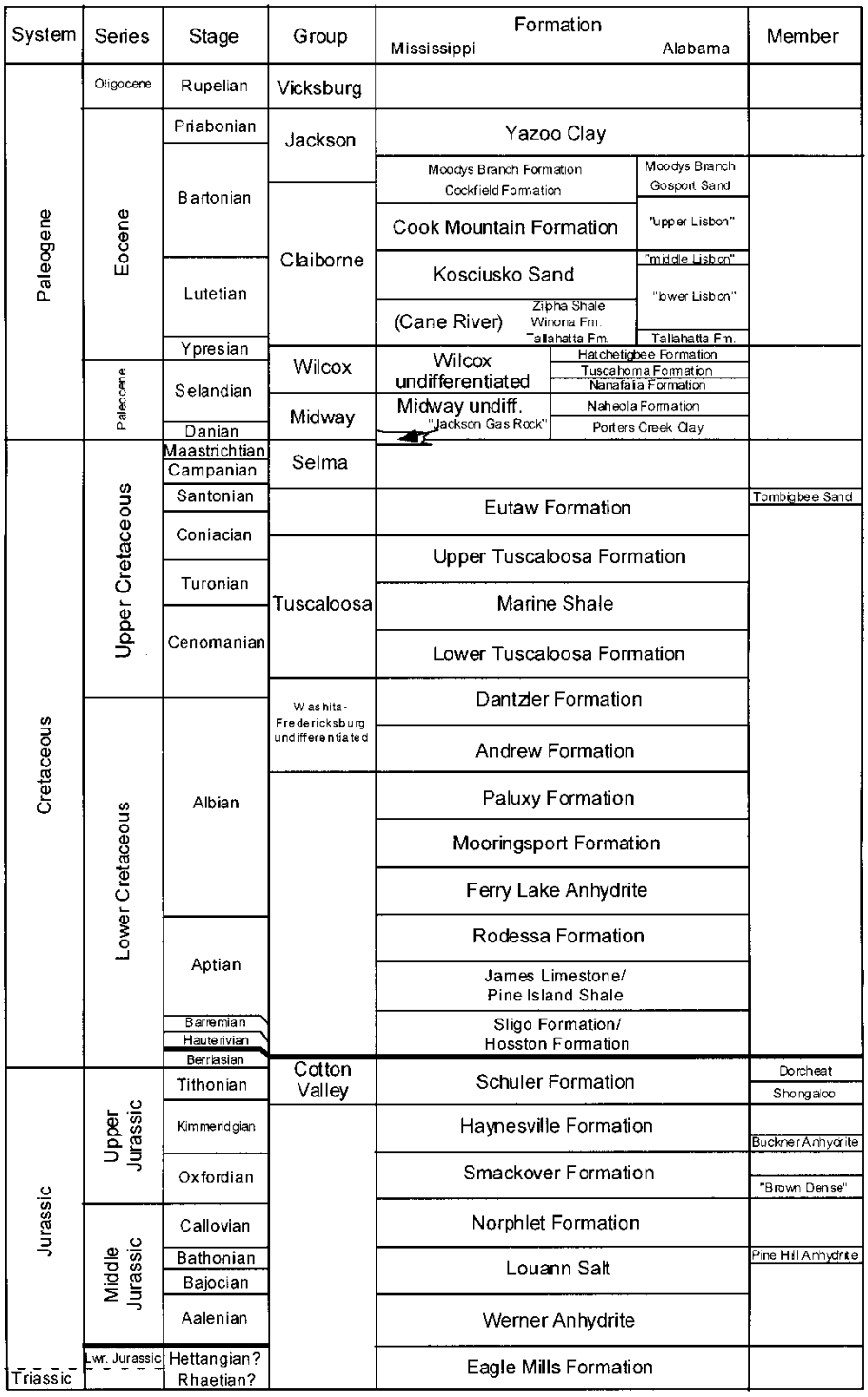

1.6 Carbon dioxide

Injection into oil-, gas-, and water-bearing lithologies is the most common option for carbon dioxide storage, and represents the only option that has been applied at the commercial scale (Rackley, 2010). The effectiveness and use of this option rely on the site characterization, the monitoring technologies, and the availability of carbon dioxide. Carbon dioxide storage requires specific geological characteristics. The presence of competent sealing boundaries, effective trapping in the target formation, the absence of vertical conduits through open faults and fractures, isolation from the surface connected aquifers, and a suitable hydrodynamic regime constitutes the different characteristics for a reservoir to be suitable for carbon dioxide (Rackley, 2010). Two possible geological settings are suggested for carbon dioxide storage: 1) storage in a saline aquifer and 2) storage in an oil or gas reservoir.

Carbon dioxide injection has been used in oil reservoirs as an enhanced oil recovery technique (EOR), particularly in the Permian Basin, Unites States (Rackley, 2010). Also, more recently, carbon dioxide has been used for EOR in the 1) Encana-operated Weyburn and 2) the Apache Canada-operated Midale in Saskatchewan (Rackley, 2010). In these two cases, the use of carbon dioxide has improved the oil recovery from 5% to 10% of the original oil in place (OOIP), varying according to reservoir characteristics and the recovery efficiency of the preceding secondary recovery phase (Rackley, 2010).

Carbon dioxide has proven to be a key element in oil recovery, however, through time it can affect the different characteristics of the reservoir including: porosity, permeability, mineralogy, and fractures. During high-pressure carbon dioxide injection in

a deep aquifer, it is possible that siderite and dolomite could be precipitated (Marini, 2007), consequently, leading to a decrease in porosity. Also, a reaction path modeling of geological carbon dioxide sequestration in a glauconitic sandstone aquifer (using the PATHARC.94) of the Alberta Sedimentary Basin, Western Canada revealed a substantial trapping of carbon dioxide upon precipitation of siderite (Gunter *et al*., 1997, 2000). However, Xu *et al*. (2000, 2004) determined, in the same sedimentary basin, that the volume of siderite precipitated during such reaction could be far less than estimated by Gunter *et al*. (1997). The problem is that Gunter (1997) used annite as a proxy for glauconite. Therefore, using the TOUGHREACT, and considering glauconite instead of annite but also adding new minerals (e.g oligoclase and illite instead of albite, anorthite, and muscovite), would have led to a slight improvement of carbon dioxide sequestration capacity (Xu *et al*., 2000, 2004). Another experiment, this time in the sediments of the Gulf Coast by means of TOUGHREACT, would have produced solid phases product such as illite, dawsonite, ankerite, calcite, and siderite, with the last two (calcite and siderite) dissolving after a period of time (Xu *et al*., 2000, 2004). In the White Rim Sandstone, using the ChemTough code, White *et al*. (2005) found that 1,000 years after the end of the injection period approximately 21% of the injected carbon dioxide would have been trapped in carbonate minerals (calcite and dawsonite), at that time, 52% would have been present underground as a separate gas phase or would have dissolved in groundwater, and 17% would have leaked to the ground surface. In the carbonate rocks of the Alberta sedimentary basin, a rapid dissolution of calcite and siderite would have been observed while dolomite would have precipitated (Gunter *et al*., 2000). Most experiments involving the impact of carbon dioxide on rocks were conducted via simulation, using

different software such as TOUGHREACT, ChemTough code, and PATHARC, etc…. However, lately few actual laboratory experiments have been conducted. The results were generally not successful because of the slow kinetics of the processes (Marini, 2007). The "few" noticeable success in laboratory experiments were conducted by Kaszuba *et al*. (2003, 2005), Pearce *et al.* (1996), Rochelle *et al.* (1996), and Sass *et al.* (1997) . After a period of respectively 80 days and 77 days and at a constant temperature of 200 degree Celsius, documentation of etching of potassic lamellae, growth of clay minerals on oligoclase, coatings of magnesite, corrosion of magnesite and euhedral siderite was recorded in the different samples (Kaszuba *et al*., 2003, 2005). Also, calcite and dolomite showed traces of alteration while dissolution of anhydrite followed by precipitation of calcite was observed by Pearce *et al.* (1996) and Rochelle *et al.* (1996). Furthermore, Pearce *et al.* (1996) and Rochelle *et al.* (1996) recorded corrosion of detrital feldspars accompanied by precipitation of Na-smectite. Further, Sass *et al.* (1997) did not record any major changes after reacting anorthite and glauconite with carbon dioxide and synthetic brine composed of Na-Ca-Cl. In the anorthite case, Ca was released in the system but precipitation of carbonate did not occurred, while in the glauconite case, an increase of Na was observed accompanied with a decrease in of K, Fe, and Si with no carbonate mineral precipitation (Sass *et al.,* 1997).

Understanding the interaction between the reservoir and carbon dioxide during sequestration and storage can provide valuable information for geologists to predict possible changes in reservoir characteristics (porosity, permeability, mineralogy, fractures) through time. Also, mineral trapping is considered as one of the most permanent methods to sequester carbon dioxide in the subsurface (Marini, 2010).

CHAPTER II

METHOD

2.1 Sample Selection

The samples for this study were obtained from the Mississippi Department of Environmental quality in Jackson, Mississippi. Approximately 3,970 to 9,610 ft (1210 to 2929 m) of cut core samples were carefully analyzed. A total of 8 standard sized (27 mm x 46 mm) samples for rectangular thin section were chosen for this study. Also, a sample of calcitic Indiana Limestone/Bedford Limestone (known formally as the Salem Formation) was provided by Dr Brenda Kirkland to be used as a control during the experiment due to the homogeneous mineralogy and pore network of the sample. Samples were also selected according to pertinent data gathered from previous research on the Cook-McCornick core, Heidelberg field (Collins, 2008).

2.2 Petrographic sectioning and standard petrographic analyses

A total of 8 samples were sent to Spectrum Petrographics, Inc; 7 samples were made into standard (27 mm x 46 mm) and 1 sample into a grain mount rectangular thin sections. Each thin section was impregnated with the blue dyed-epoxy with no cover slips attached to facilitate the identification of porosity and porosity types, fractures, and enlarged fractures present. Petrographic analyses were carried out by observing each thin section under a standard Olympus BX50 petrographic microscope under transmitted

light. Photomicrographs of porosity, minerals, fractures, and cements present were taken using a Nikkon Coolpix 990 digital camera, before and after exposure to carbon dioxide.

2.3 Scanning electron microscopy (SEM) analyses

A portion of the samples was selected for SEM analyses. SEM was used to determine the nature of the pore systems and minerals present in each samples. Each selected, freshly broken sample for SEM analyses was Au/Pd coated using the polaron SEM coating system, for about 30 seconds in order to gain the required electrical conductivity.

Elemental compositions within observed samples were also examined using the attached X-ray Electron dispersive (X-EDS) spectrometer of the JEOLJSM-6500F Field emission Scanning Electron Microscope (FESEM). High resolution pictures of observed features were acquired with the FESEM's digital image system. All SEM analyses were carried out at the Mississippi State University Institute for Imaging and Analytical Techniques (I^2AT).

2.4 X-ray diffraction (XRD)

A fraction of each sample was carefully obtained with a dental instrument and ground to fine powder with a mortar and pestle. A portion of the finely ground powder was put on a glass slide that was inserted into the horizontal stages with a measuring range of 3° degrees to 70° degrees 2θ. Appropriate settings were utilized and each powder sample was analyzed in the Rigaku XRD system for at least 180 minutes. The exact mineralogy of the sampled powder was confirmed using the Jade® XRD analytical software. XRD was used to confirm the mineralogy present (quartz, feldspars, calcite,

dolomite, glauconite, etc….) in each of the eight samples before and after exposure to carbon dioxide. XRD analyses were performed at Mississippi State University (I^2AT).

2.5 Porosity analyses

Porosity percent averages were determined on the thin sections of each of the 8 samples (White et al., 1998), before and after exposure to carbon dioxide. Porosity was determined by the means of point count technique, using the standard Olympus BX50 petrographic microscope under cross-polarized light. Point count was performed by determining the presence or absence of porosity at points on a grid spaced 1 mm apart. Once the top or bottom of the sample was reached, the sample was moved 1 mm to the left and the process was performed again. A total of approximately 100 to 300 point counts were conducted for the 8 samples. Also, in the attempt to verify the data generated by the mean of point count, Jpor analysis was performed on the pre-carbon dioxide sample. Jpor is freeware that determines average porosity in thin section by calculating the amount of pixels that are blue as a result of epoxy filling pore spaces. Jpor was obtained online at www.geoanalysis.org/jPor.htlm. Each thin section was digitized using the HP Deskjet 2050 J510 series scanner. The images obtained were then altered to re-enforce the shades of blue representing porosity in the thin sections, then saved as a TIFF file, the only file type recognizable by the freeware. ImageJ was then used to find the number of pixels of each shade of blue known to represent porosity. The total sum of pixels determined as porosity in each thin section is divided by the total number of pixels in the whole image to give the average porosity.

2.6 Carbon dioxide test

Carbon dioxide solution was prepared using reverse osmosis water (RO) with a pH of 7. Reverse osmosis water was used to ensure and minimize the presence of any chemicals (fluoride, chlorine, chloramines, nitrates, etc…) or metals in the water. Using a diffuser, carbon dioxide was added and dissolved in the water, making a carbonic acid solution (equation 2.1).

$$CO_{2(g)} + H_2O \rightleftharpoons CO_{2(aq)} + H_2CO_3 \quad (2.1)$$

The eight samples were impregnated with the carbonic acid solution and inserted in core tube apparatus (fig 2.1), designed by Dr. Lewis R. Brown of the Department of Biological Sciences at MSU to hold incubating samples under constant pressure. The core tubes were inserted in the QL Model 10 Lab Oven, at an initial Temperature of approximately 30° to 35° degrees Celsius then raised up to 80°-90° degrees Celsius for a total period of six months (182 days). The carbon dioxide test was conducted in Hilbun Hall biogeochemistry laboratory, Department of Geosciences, Mississippi State University.

Figure 2.1 Core incubation apparatus designed by Dr. Brown. Apparatus able to simulate high pressure, high temperature subsurface conditions for tests on small core samples.

2.7 Focused Ion Beam Tomography (FIB-SEM)

A Focused Ion Beam-SEM (FIB) was used to prepare cross-sections for Sample 8 (dolomitic-Limestone/Smackover Fm). The multiple cross-sections, created by the FIB-SEM, were used to investigate pore connectivity and the distribution of the possible precipitation of new mineral within the pore system after carbon dioxide treatment. Also, a 3D reconstruction of the microstructure using images generated by FIB-SEM before and after treatment was generated. The sample was attached to an aluminum stub with silver paste, and then was introduced in the Auriga 60 Zeiss system. The area of study was approximately 20 by 20 micron. A metal plate was mounted on the area interest with intent to avoid and at the same time delineate the area to be studied. The sample was then tilted at an angle of around 52° degree allowing direct observation of the prepared section. FIB was then used to remove a 10 nm thick cross-section face. Image of each cross-section faces removed was imaged. The process was repeated 500 to 600 times, creating a 3D data set of the dolomitic-limestone microstructure. All FIB analyses were

performed at the Joint School of Nanoscience and Nanoengineering (JSNN), in Greensboro, North Carolina.

CHAPTER III

RESULTS (PRE AND POST CARBON DIOXIDE)

3.1 Sample selection

Approximately 5,640 ft (1719 m) of cut core samples from the Heidelberg field were observed and from that six samples were taken for analysis. The types of lithology described include dolomitic-limestone, sandstone, and shaly-sandstone. Six samples from a total of eight for the study were chosen from the Heidelberg field and associated with a specific formation using depth or a specific lithology (table 3.1). Actual samples Location were proprietary, thus associating the exact depth to each formation was based on log data and structural map. Porosity trend, grain types, and mineralogy for all the samples were generally assessed and included in the thin section petrographic analysis section. Diagenetic features present in the sandstone and shaly-sandstone were mostly fractures (fig 3.1) and oil remnants; while in the dolomitic-limestone and limestone, fractures were mostly observed. Table 3.1 shows a brief initial description of the eight samples.

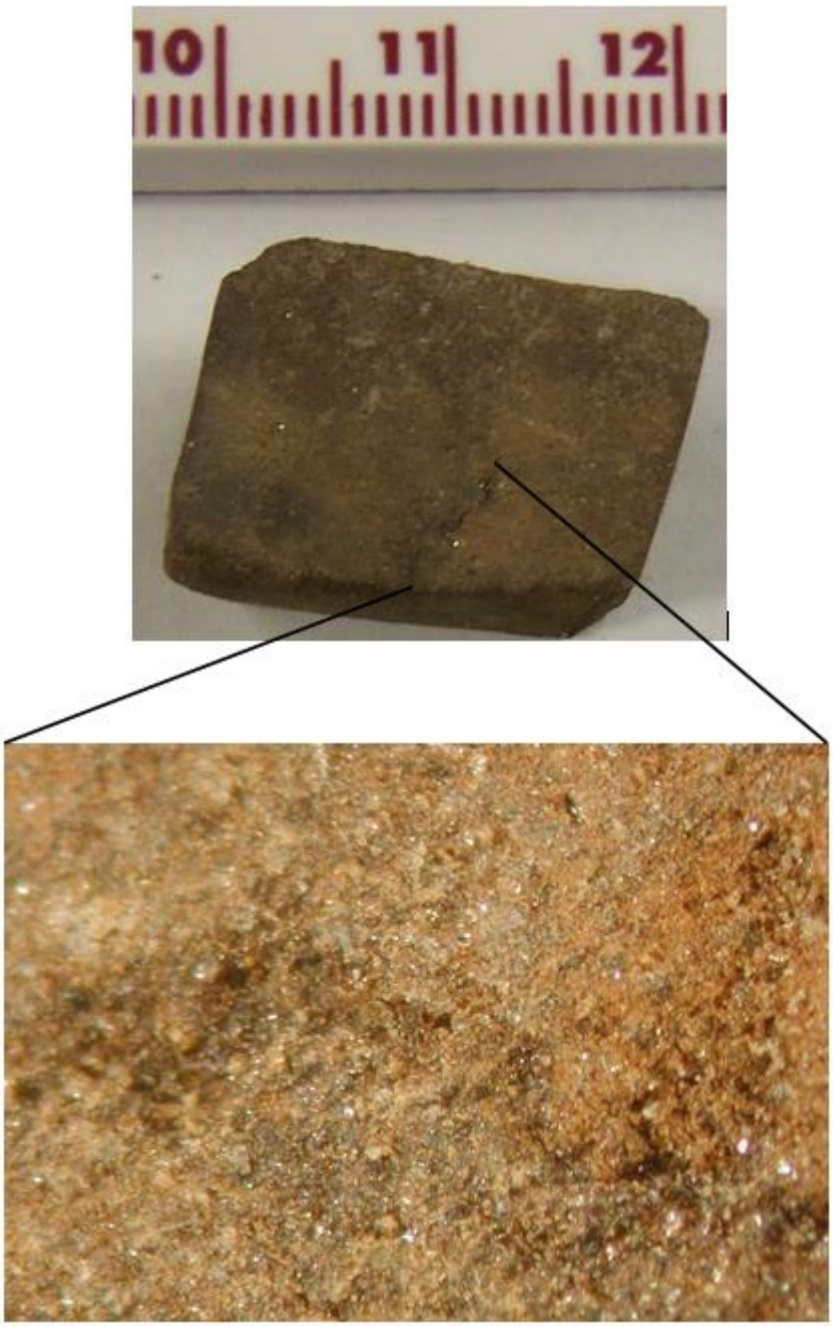

Figure 3.1 Sun-7 (Sandstone/Heidelberg field)-8410-8787’ ft

Picture shows possible enlarged fracture (pre-carbon dioxide).

Table 3.3 Cut core sample descriptions for the eight samples selected for the study

Sample	Sample Depth	Lithology	Diagenetic Features	
			Fractures/enlarge fracture	Oil remnants
St-1	4916-5581 ft	Shaly-sandstone	No	No
Sc-2	Salem control	Limestone	No	No
Ssm-3	15231-15286 ft	Sandstone	No	Yes
Ssm-4	15281-15286 ft	Sandstone	No	No
Se-5	4774.5' ft	Shaly-sandstone	No	Yes
Se-6	4709' ft	Sandstone	No	No
Sun-7	8410-8787' ft	Sandstone	Yes	No
S-8	Core	Dolomitic-limestone	Yes	No

Six samples were associated with the Heidelberg field. The Smackover core sample was cut off of a teaching sample donated to Dr. Brenda Kirkland by Mobil Oil Corporation,from an unknown locality and the sample of the Salem Formation was donated to Dr. Kirkland by the Indiana State Geological Survey and was used as a control sample during the experiment.

3.2 Thin Section Porosity Results

Porosity average was determined pre- and post- carbon dioxide exposure in a total of eight samples by using the point counting method. The quantified porosity for each thin section was plotted and a porosity graph correlating each sample was generated. Also, the average porosity, pre-carbon dioxide, was quantified using thin section digitized images (fig 3.2). The thin sections post carbon dioxide were not dyed with blue epoxy, so making it impossible to use the Jpor freeware. The values for pixel counts associated with porosity (shades of blue) as well as the total amount of pixels for each thin section and

point count data in percent are showed in Table 3.2. Figure 3.3 and 3.4 represent porosity percent analyses and trend for all the samples from the Heidelberg field pre- and post carbon dioxide.

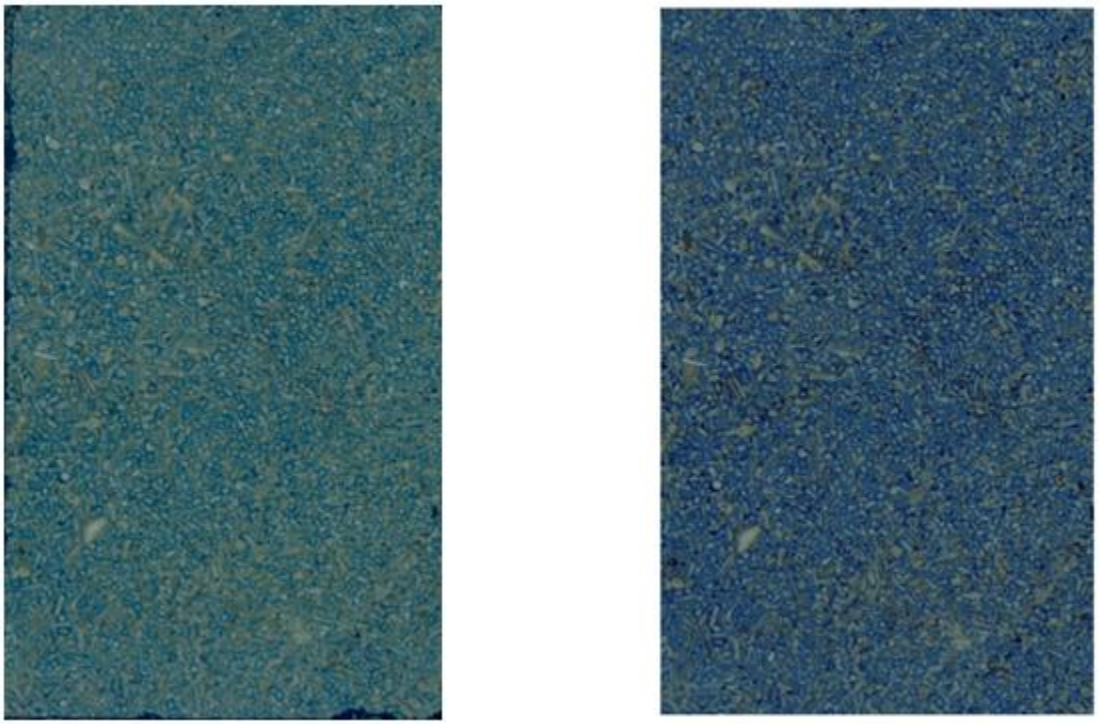

Figure 3.2 Left represents scanned image of thin section – right represents image after contrast enhancement for porosity determination.

Table 3.4 Pixel counts for Thin Section Porosity analyses pre- and post- carbon dioxide.

Samples	Depth	Pixel counts (Pore spaces)	Total pixel counts	Pre-carbon dioxide porosity (Jpor)	Pre-carbon dioxide porosity (Point counts)	Post-carbon dioxide porosity (Point counts)
St-1	4916-5581 ft	153897	2821879	5.4537 %	4 %	5 %
Sc-2	Salem control	1094602	3733488	29.3185 %	23 %	26 %
Ssm-3	15231-15246 ft	14912	2712477	0.5498 %	1 %	1 %
Ssm-4	15281-15286 ft	372	3263750	0.0114 %	0 %	0 %
Se-5	4774.5' ft	2590	2651716	0.09767 %	0 %	1 %
Se-6	4709' ft	86865	2557152	3.3969 %	5 %	0 %
Sun-7	8410-8787' ft	11219	3187350	0.352 %	1 %	2 %
S-8	Core	3894	2856340	0.1363 %	1 %	1 %

Pixel counts, total pixel, and percent porosity generated by Jpor analysis for pre-carbon dioxide samples were included in the table as a mean of comparison (statistical analysis by permutation shows a *P*-number of 0.8739).

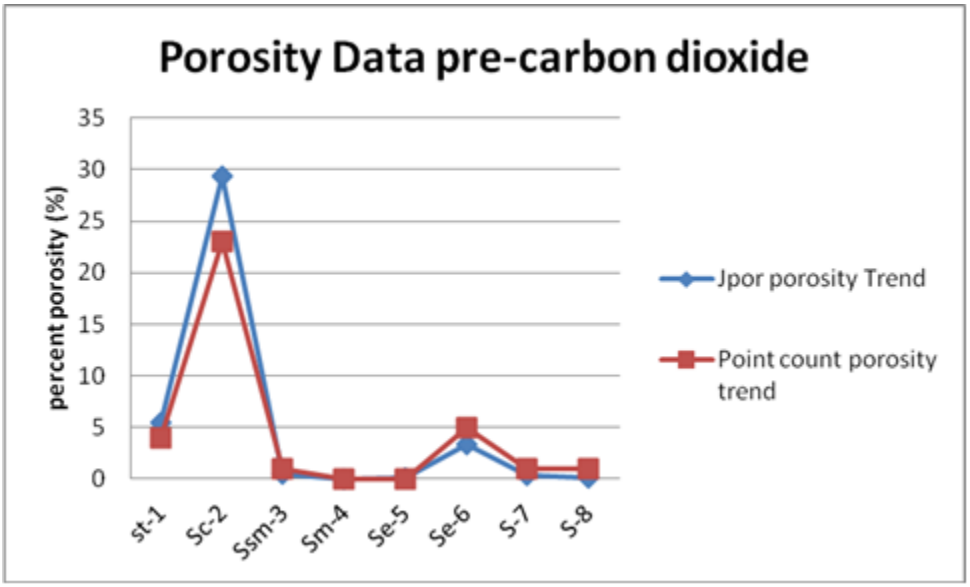

Figure 3.3 Graph showing the percentage of porosity measured with two different methods.

Blue line shows porosity data for each sample generated using Jpor method while the red plot shows porosity data using the point count method. Statistical validity of porosity data using Jpor and point count was verified using the permuation method (*P*-value: 0.8739).

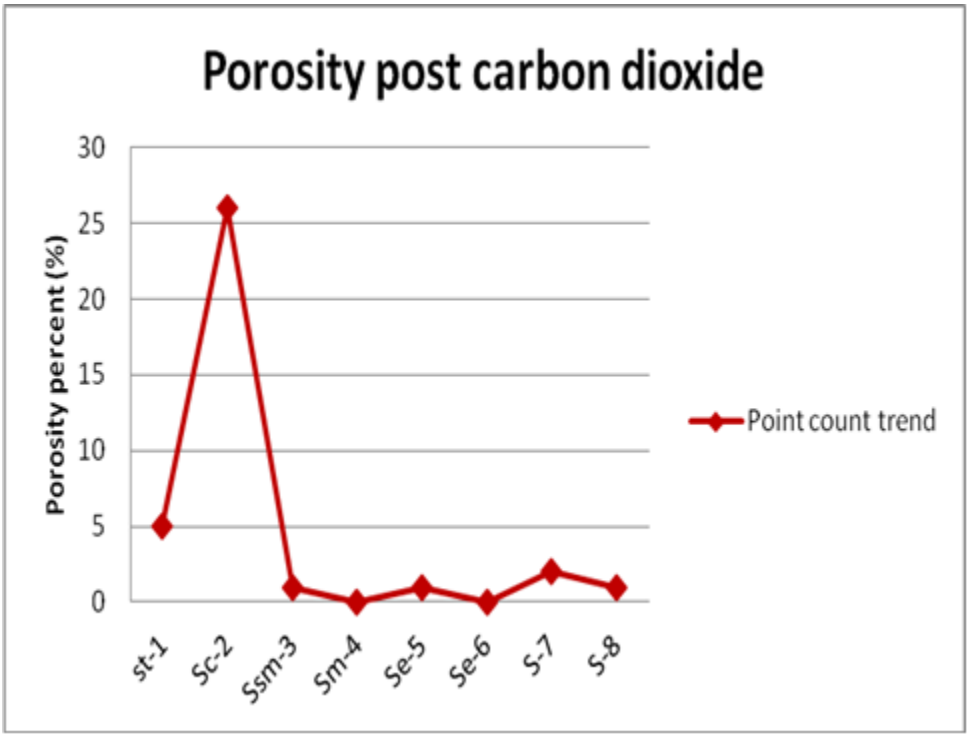

Figure 3.4 Graph shows porosity trend for each sample after carbon dioxide treatment

3.3 Petrographic analyses Results

A total of 7 standard (27 mm X 46 mm) and 1 grain mount rectangular thin sections were prepared and analyzed in this study. A Total of 6 thin section slides were made from samples obtained from cores, core plugs, and cuttings taken from wells in the Heidelberg field. In addition, two samples were obtained from Dr Brenda Kirkland, one of which was used as control because it is known to be composed of predominantly of calcite. Pictures of the eight thin section slides were taken with a petrographic microscope and types of porosity, microfractures, minerals, and lithostratigraphy were determined pre and post carbon dioxide treatment. Furthermore, petrographic analysis was conducted to record and document any possible changes such us: alteration, precipitation, and porosity.

3.3.1 Sample 1- St-1- Heidelberg field/4916-5581 ft

St-1 is characterized by multiple cuttings. Thin section was made by grain mount. Fractures present must be artifacts. Pre-carbon dioxide analysis unveiled that quartz grains are dominant and embedded in calcite cement. Grain size varies from 1.00 to 0.25 mm. Also, presence of glauconite and calcite minerals can be noted in calcite cement. Further, shells of gastropods were noted but seem to have been replaced by calcite. Porosity was determined to be of vuggy nature, interparticle, and intraparticle. Post-carbon dioxide treatment analysis shows evidence of possible dissolution in calcitic gastropod shells. Figure 3.5 shows quartz (white and gray) and glauconite (green) in calcite cement, Figure 3.6 shows vuggy porosity (dark, irregular shapes that cross cut allochems), calcitic shell fragments and clasts, quartz grains, and an intraclast (brown, lower right) in a micrite matrix in pre carbon dioxide sample. Figure 3.7 and 3.8 are showing possible dissolution in both clay and calcite after carbon dioxide treatment.

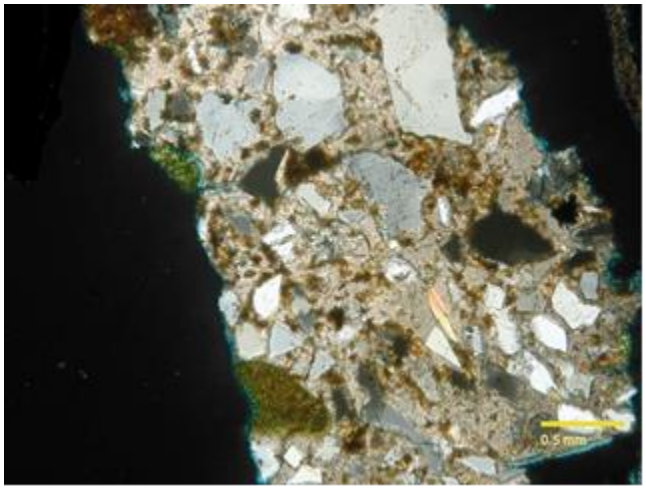

Figure 3.5 St-1 4916-5581 ft Photomicrograph shows quartz (white and gray) and glauconite (green) in calcite cement (pre-carbon dioxide treatment).

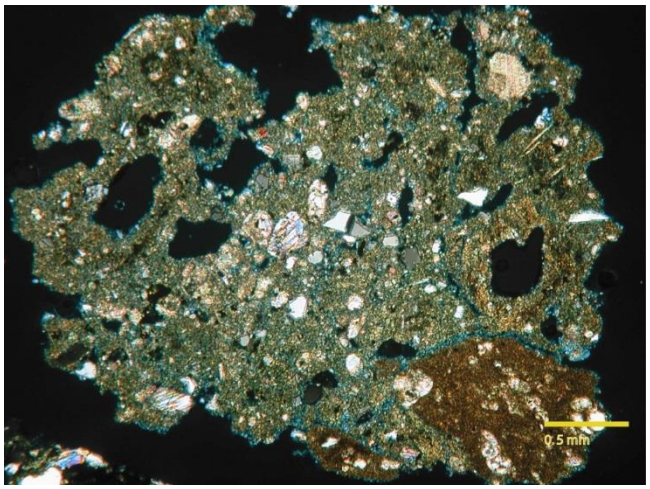

Figure 3.6 St-1 4916-5581 ft Vuggy porosity (dark, irregular shapes that cross cut allochems), calcitic shell fragments and clasts, quartz grains, and an intraclast (brown, lower right) in a micrite matrix (pre-carbon dioxide treatment).

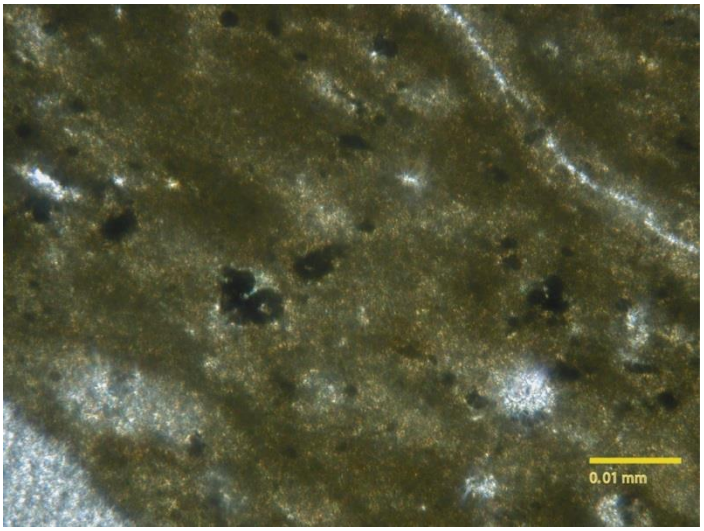

Figure 3.7 St-1 4916-5581 ft- Photomicrograph showing possible dissolution in clay (post-carbon dioxide).

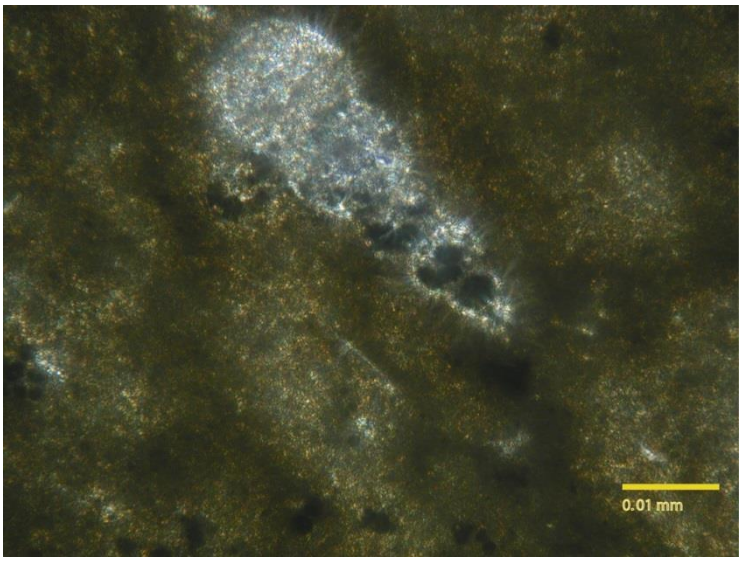

Figure 3.8 St-1 4916-5581 ft- Photomicrograph showing possible evidence of dissolution in calcite.

Mineral replacement of gastropod shell (post-carbon dioxide).

3.3.2 Sample 2- Sc-2- Limestone-Salem Formation (control)

Sc-2 represents a pure limestone from the Salem Formation (Indiana) and was used as a control during the experiment. Sc-2 is characterized by abundant presence of oolitically coated bryozoans' fragments, foraminifera fragments filled with micrite. The cement was determined to be calcite. Two types of cement can be identified: syntaxial and meteoric calcite. The size of the different allochems present varies from 1.00 to 0.50 mm. The types of porosity present include interparticle, intraparticle, and microporosity. Pre-carbon dioxide analysis shows in Figure 3.9 allochems including oolitically coated bryozoan fragments, coated and uncoated echinoderm fragments, and possible foraminifera fragments all interspersed with interstitial micrite cemented by syntaxial calcite. Figure 3.10 shows syntaxial calcite cement with partially developed twin lamellae, the dominance of blue shows significant porosity and micro porosity within the

micritic component of sample. Post-carbon analysis revealed possible dissolution of calcite. Also, the presence of spalling due to overburden was recorded. Figure 3.11 shows possible dissolution of calcite cement and Figure 3.12 spalling due to pressure from overburden.

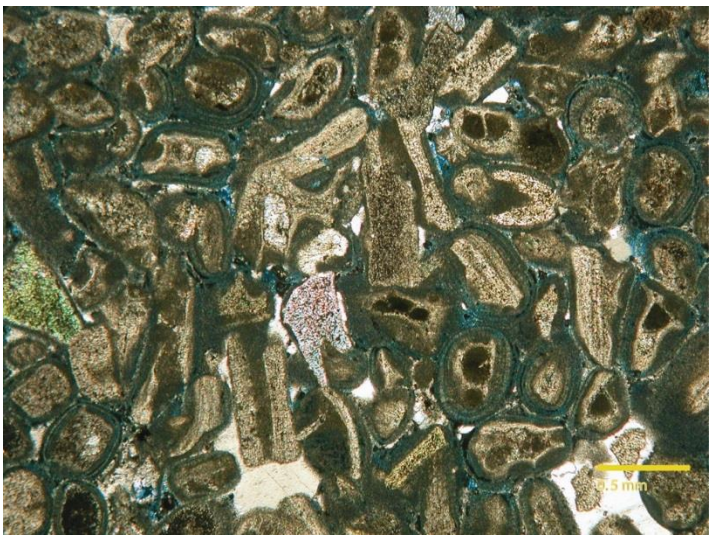

Figure 3.9 Sc-2- Limestone (Salem Formation) Photomicrograph showing oolitically coated bryozoan fragments, coated and uncoated echinoderm fragments, and possible foraminifera fragments with interstitial micrite and syntaxial calcite cement in the Salem Limestone used as a control because it is predominantly calcite (pre-carbon dioxide).

Figure 3.10 Sc-2- Limestone (Salem Formation) Syntaxial calcite cement with partially developed twin lamellae.Dominance of blue shows significant porosity and micro porosity within the micritic component of sample (pre-carbon dioxide).

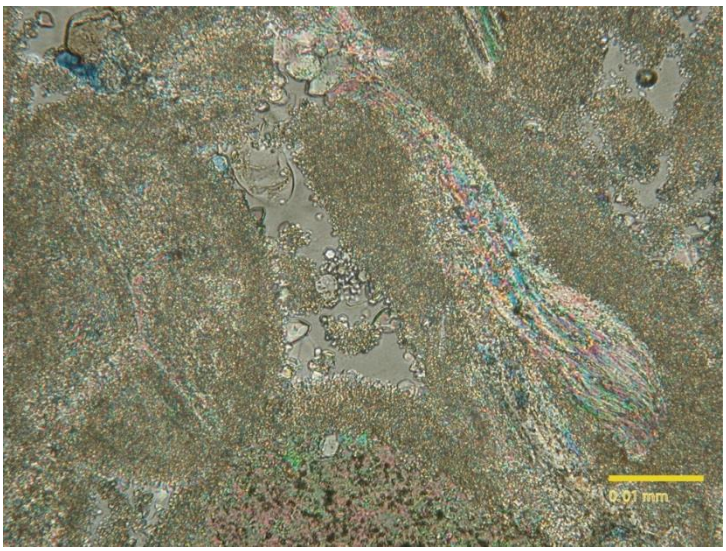

Figure 3.11 Sc-2- Limestone (Salem Formation) Photomicrograph shows possible dissolution of calcite cement in the upper right hand corner (post-carbon dioxide).

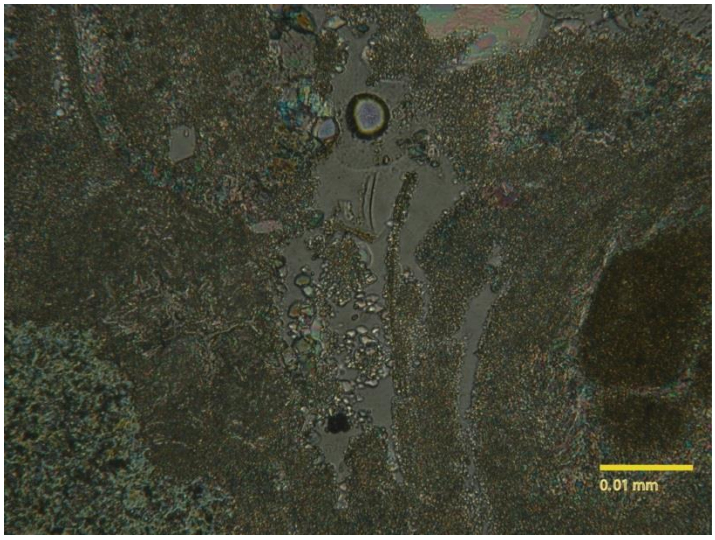

Figure 3.12 Sc-2- Limestone (Salem Formation) Spalling due to pressure from overburden (post-carbon dioxide).

3.3.3 Sample 3- Ssm-3- Sandstone- Heidelberg field- 15231-15246 ft

Ssm-3 was classified as sandstone and characterized by the abundance of quartz grains and muscovite as an accessory mineral. Quartz grains are angular to sub angular with size varying from coarse to medium sand. The sample is moderately sorted with principal cement to be clay. Also, possible presence of dead oil within pores is to be noted. Pre-carbon dioxide analysis shows in Figure 3.13 partially altered muscovite replaced by quartz and Figure 3.14 shows oil remnants within micro fracture. Post-carbon dioxide unveiled possible dissolution in microcline Figure 3.15 and Figure 3.16 shows enlarged fracture and uncompacted quartz grains supported within matrix.

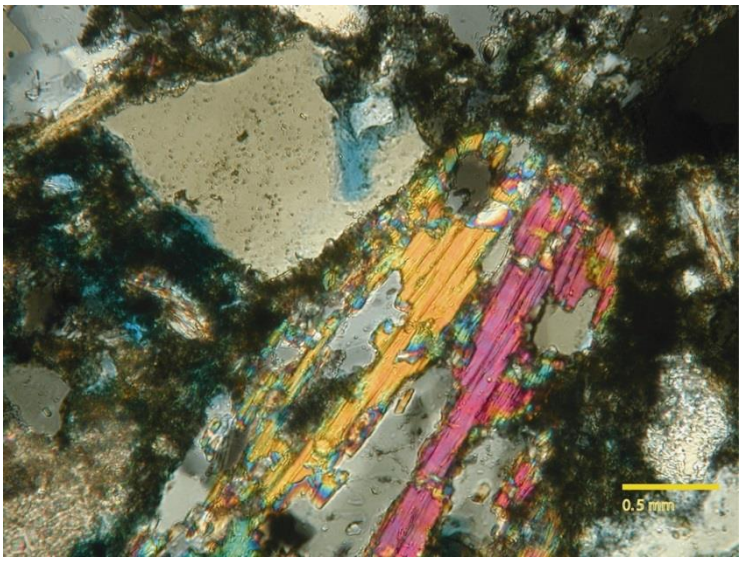

Figure 3.13 Ssm-3- Sandstone (Heidelberg field)- 15231-15246 ft Muscovite altered and partially replaced by quartz in clay matrix (pre-carbon dioxide).

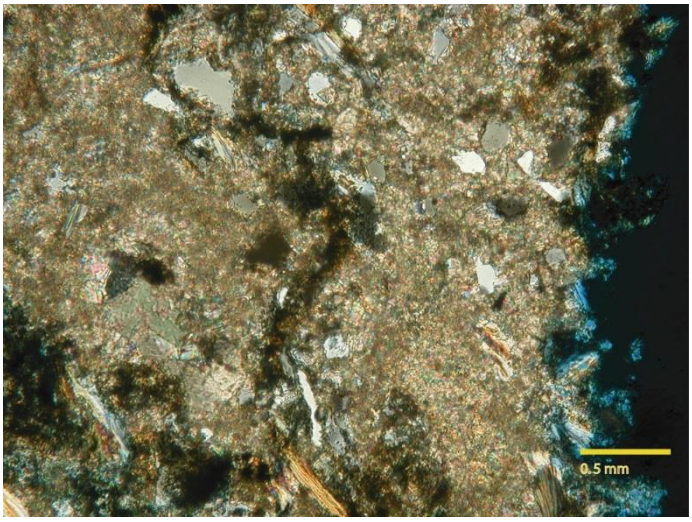

Figure 3.14 Ssm-3- Sandstone (Heidelberg field) 15231-15246 ft Elongate brown zone in center is possible oil remnant within microfracture and margin of a vuggy pore on far right (pre-carbon dioxide).

Figure 3.15 Ssm-3- Sandstone (Heidelberg field)- 15231-15246 ft Photomicrograph shows voids in grain, possibly dissolution features and also note fracture on left corner. Arrows point to dissolved microcline (post-carbon dioxide).

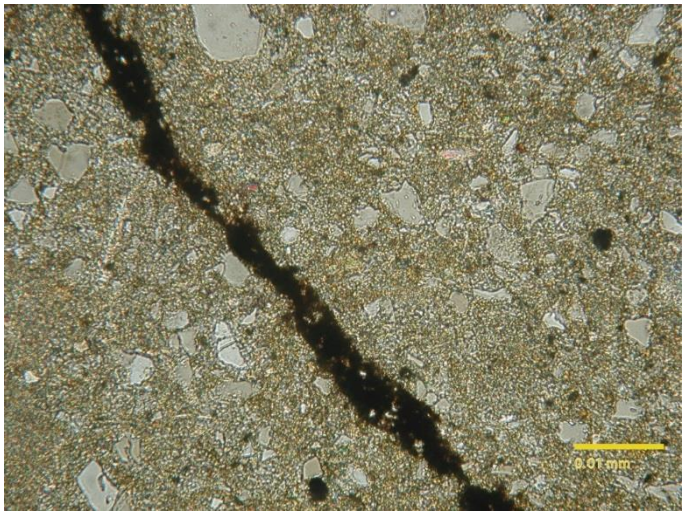

Figure 3.16 Ssm-3- Sandstone (Heidelberg field)- 15231-15246 ft Photomicrograph shows enlarged fracture, and uncompacted quartz grains supported within matrix (post-carbon dioxide).

3.3.4 Sample 4- Ssm-4- Sandstone- Heidelberg field- 15281-15286 ft

Ssm-4 is a sandstone from the Heidelberg field and made up of poorly sorted quartz grains embedded in a hematite matrix. Quartz grains size vary from fine to coarse and are angular to sub-angular shape. Porosity distribution is irregular and includes mostly interparticle porosity. Figure 3.17 shows quartz within hematite matrix and Figure 3.18 shows irregularly distributed interparticle porosity pre-carbon dioxide. Post-carbon dioxide analysis shows little variation. However, possible alteration of quartz can be noted in Figure 3.19.

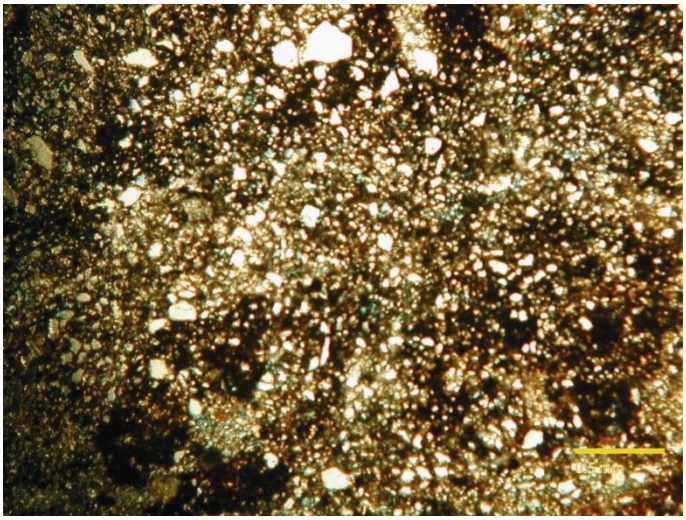

Figure 3.17 Ssm-4 Sandstone (Heidelberg field)- 15281-15286 ft Photomicrograph of quartz and possible hematite matrix. Scale bar is 0.5 mm long (pre-carbon dioxide).

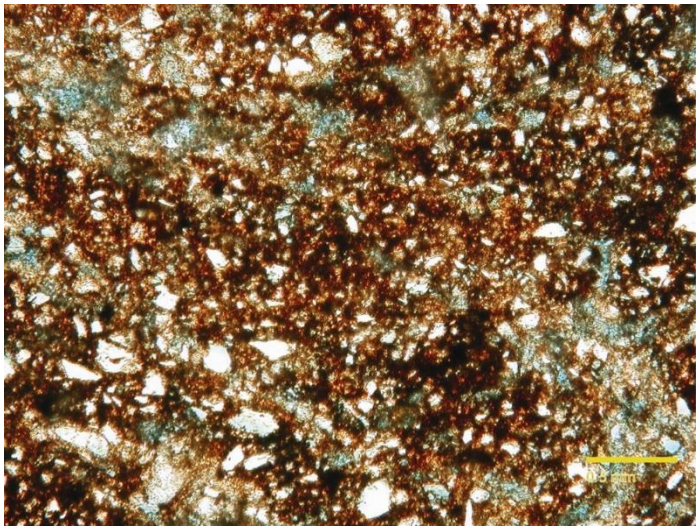

Figure 3.18 Ssm-4 Sandstone (Heidelberg field)- 15281-15286 ft Irregularly distributed interparticle porosity (pre-carbon dioxide).

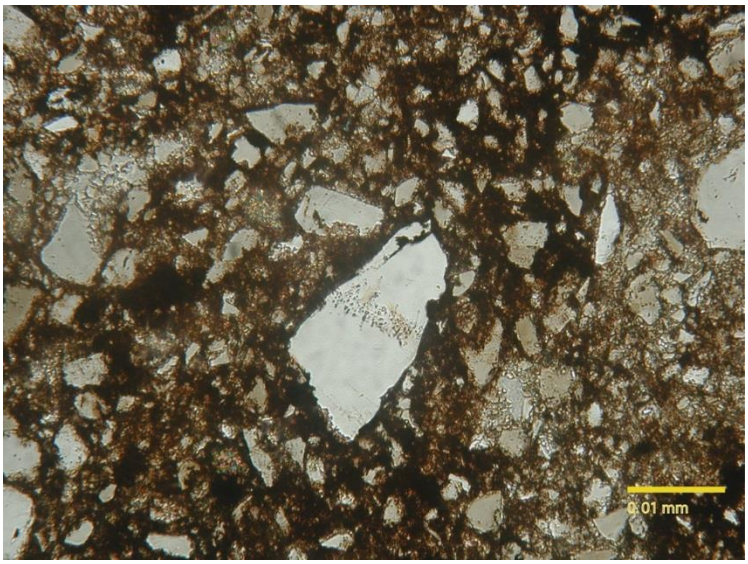

Figure 3.19 Ssm-4 Sandstone (Heidelberg field)- 15281-15286 ft Photomicrograph shows possible alteration of quartz (post-carbon dioxide).

3.3.5 Sample 5- Se5- Shaly-sandstone-Heidelberg field- 4774.5' ft

Sample 5 (Se-5) is characterized by tightly packed sand grains dominated by quartz grains with remaining minerals being muscovite, glauconite, pyrite, and possibly siderite. Quartz grains are angular to sub-angular and moderately sorted. Grain size varies from very coarse to coarse. Also, few grains of partially dissolved muscovite were present. Clay seems to be the main cement and porosity present is mostly interparticle. Pre-carbon dioxide analysis shows in Figure 3.20 quartz and muscovite. Figure 3.21 shows glauconite and possibly siderite. Post- carbon analysis of Se-5 provided evidence of new elements, which one was unidentifiable in Figure 3.22.

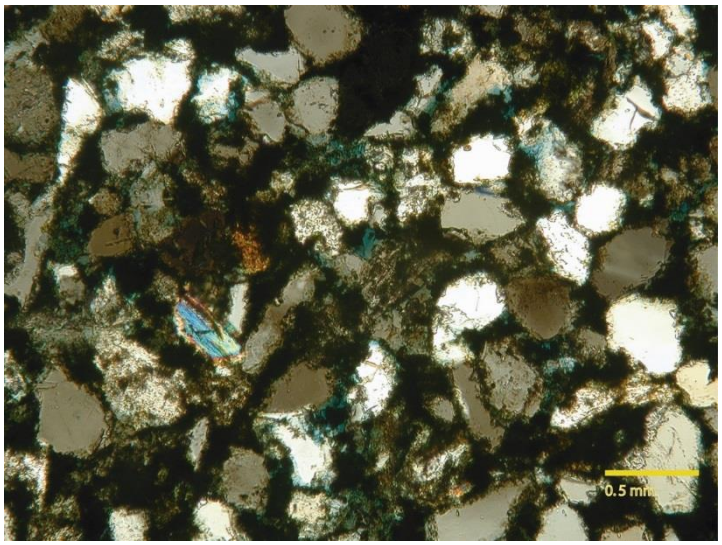

Figure 3.20 Se5- Shaly-sandstone (Heidelberg field)- 4774.5' ft- Photomicrograph showing quartz and muscovite (pre-carbon dioxide).

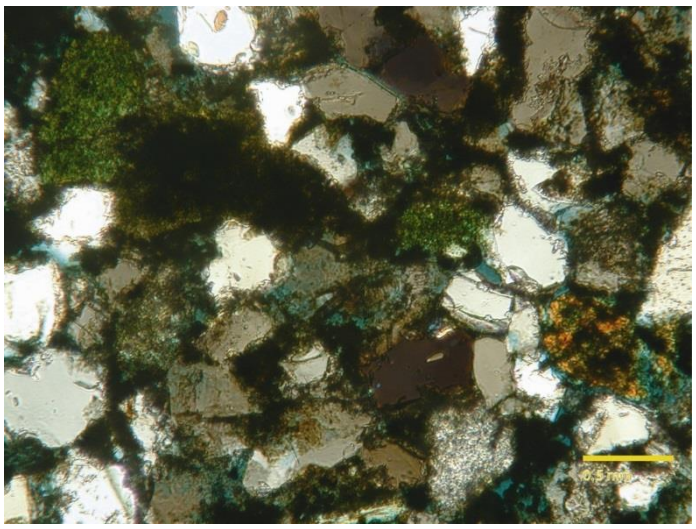

Figure 3.21 Se5- Shaly-sandstone (Heidelberg field)- 4774.5’ ft- Glauconite (green) and siderite (yellow) (pre-carbon dioxide).

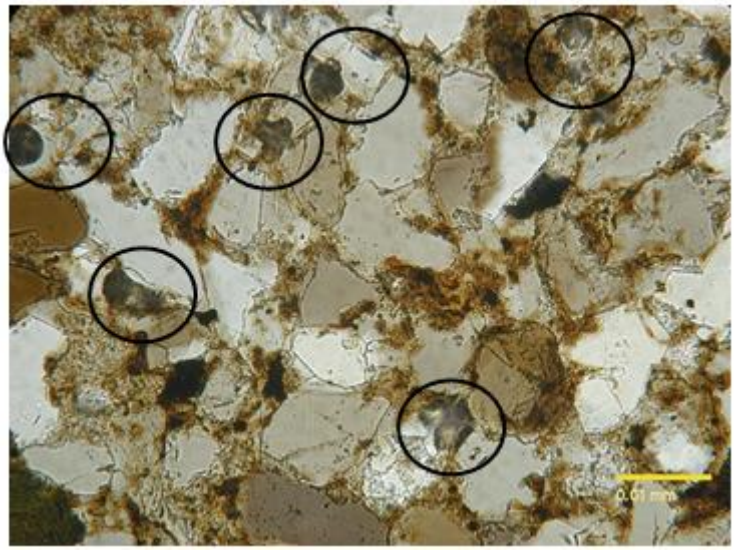

Figure 3.22 Se5- Shaly-sandstone (Heidelberg field)- 4774.5’ ft- Photomicrograph shows unidentifiable elements, possibly partially formed “gypsum”(post-carbon dioxide).

3.3.6 Sample 6- Se-6- Sandstone-Heidelberg field- 4709’ ft

Se-6 was characterized as poorly, well packed sandstone. Sample is dominated by quartz grains with presence of muscovite and glauconite as accessories minerals. Quartz grains are sub-angular and show slight trace of alteration. Grain sizes were approximately coarse to medium size. Matrix is represented by clay. Porosity type mainly included interparticle porosity. Figure 3.23 illustrates poorly sorted, well packed quartz, muscovite, clay matrix, and interparticle porosity and Figure 3.24 a close up of glauconite pre-carbon dioxide treatment. No apparent change was recorded post-carbon dioxide treatment. However, quartz overgrowth, muscovite, and brownish siderite crystalline background was observed in Figure 3.25.

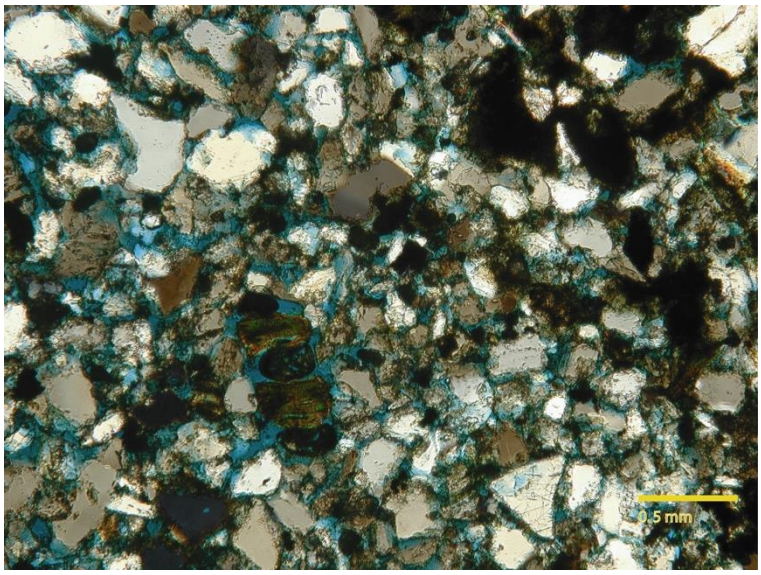

Figure 3.23 Se-6- Sandstone (Heidelberg field)- 4709’ ft Poorly sorted, well packed quartz,muscovite, clay matrix, and interparticle porosity (pre-carbon dioxide).

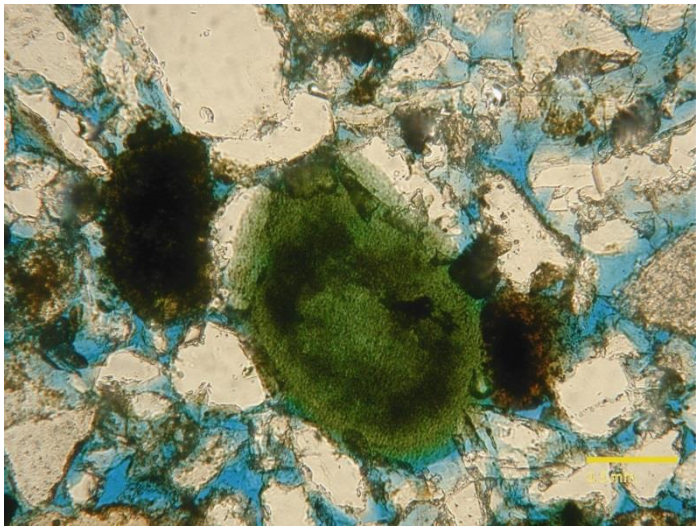

Figure 3.24 Se-6- Sandstone (Heidelberg field)- 4709’ ft Enlarged picture of glauconite; scale bar is 0.5 mm (pre-carbon dioxide).

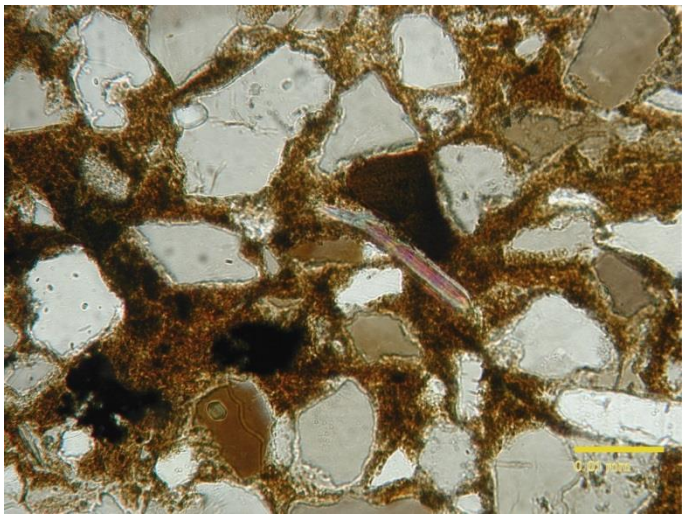

Figure 3.25 Se-6- Sandstone (Heidelberg field)- 4709’ ft Quartz overgrowth, muscovite, and brownish siderite crystalline background (post-carbon dioxide).

3.3.7 Sample 7- Sun-7- Sandstone-Heidelberg field- 8410-8787' ft

Sample 7 (Sun-7) is made up of well packed, moderately sorted to well sorted, angular quartz grains. Muscovite flakes are also present and well packed. Muscovite flakes show elongated shape. All grains are embedded in a dark matrix, flocculated clays. Porosity is relatively low and sparsely distributed within particles. Figure 3.26 illustrates quartz grains, muscovite flakes, and dark-flocculated clay matrix pre-carbon dioxide treatment. Figure 3.27 shows a magnified section of figure 3.26. Post-carbon analysis of sample 7 (Sun-7) did not show any apparent changes. Figure 3.28 shows poorly sorted quartz grain embedded in clay matrix; grain size varies from medium to coarse. Pores are filled with possible hydrocarbon remnants.

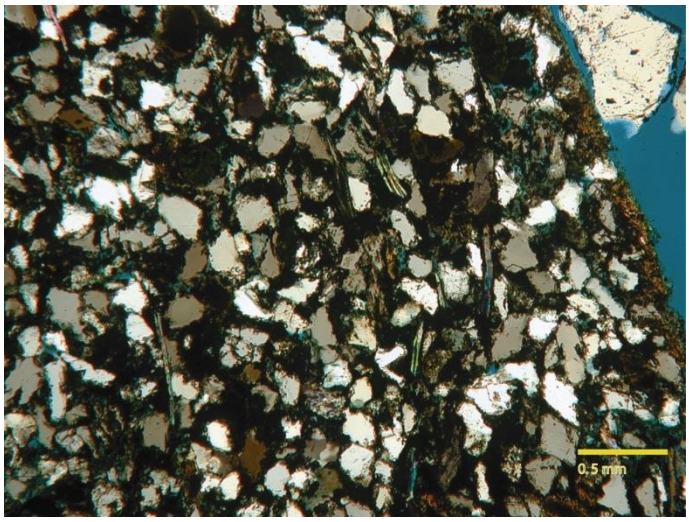

Figure 3.26 Sun-7- Sandstone (Heidelberg field)- 8410-8787' ft Picture shows well packed angular, moderately well sorted quartz grains, muscovite flakes well packed with a dark-flocculated clay matrix (pre-carbon dioxide).

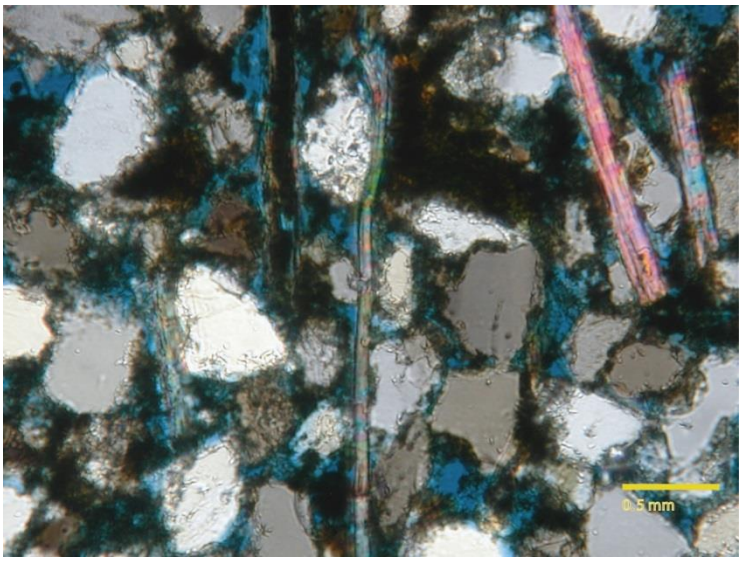

Figure 3.27 Sun-7- Sandstone (Heidelberg field)- 8410-8787' ft Magnified section of figure 3.26 showing mica flakes, some partially dissolved (center left) and interparticle porosity, blue (pre-carbon dioxide).

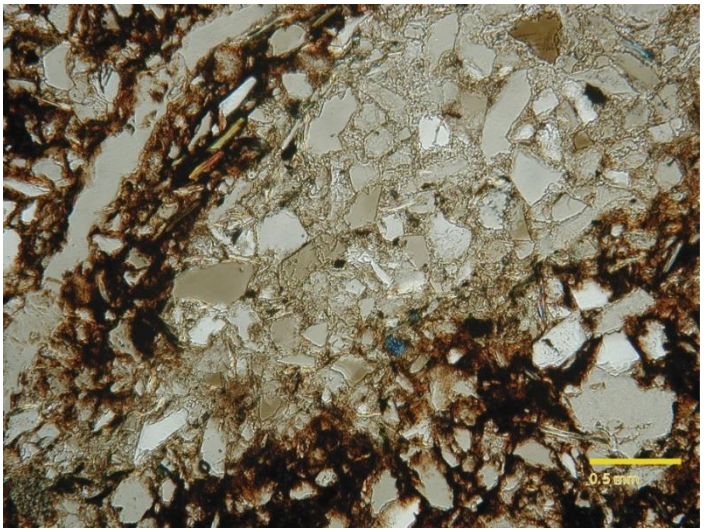

Figure 3.28 Sun-7- Sandstone (Heidelberg field)- 8410-8787' ft Picture shows poorly sorted quartz grain embedded in clay matrix; grain size varies from medium to coarse. Pores are filled with possible hydrocarbon remnants, which exhibits a dark brownish color in reflected light (post-carbon dioxide).

3.3.8 Sample 8- S-8- Dolomitic-Limestone-Smackover core

Sample 8 represents the Smackover formation. The sample used for this study is from an unknown location. The sample is characterized by the presence of calcite minerals, dolomite rhombs, and few sparsely distributed pyrites, all embedded in a calcitic matrix. Sample 8 from the Smackover formation Sample 8 from is illustrated in Figure 3.29, which shows calcite and dolomite minerals, evidence of calcite matrix and distinct dolomite rhombs pre-carbon dioxide treatment. Thin section analysis post-carbon dioxide of sample 8 did not show any evidence of change; however, presence of pyrite was confirmed. Figure 3.30 shows pyrite surrounded by dolomite.

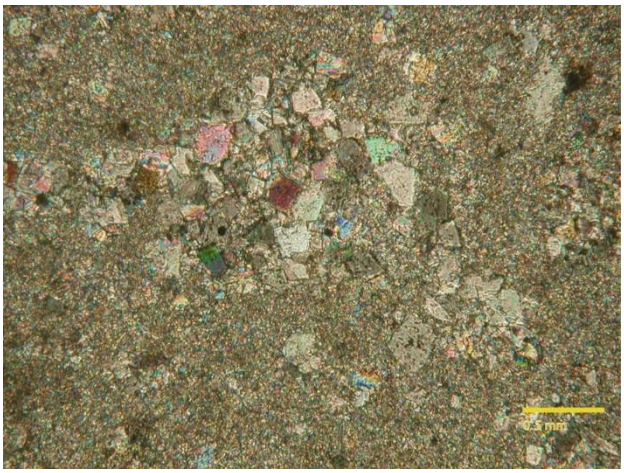

Figure 3.29 S-8- Dolomitic-limestone (Smackover core) Picture shows calcite and dolomite minerals, evidence of calcite matrix and distinct dolomite rhombs (pre-carbon dioxide treatment).

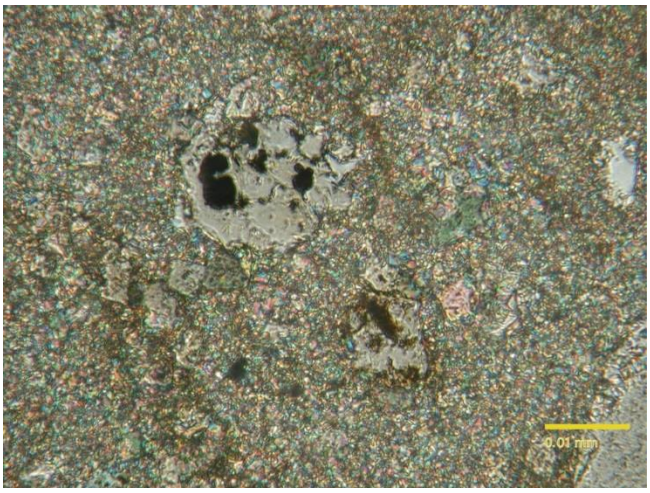

Figure 3.30 S-8- Dolomitic-limestone (Smackover core) Picture shows pyrite surrounded by dolomite (post-carbon dioxide treatment).

3.4 X-Ray Diffraction Results

XRD analyses were conducted to determine and confirm the mineralogy before and after exposure to carbon dioxide in all samples. The XRD results for all the samples are recorded in table 3.3. Little to no variation was recorded in the most of the samples, however, sample (Sun-7) shows presence of muscovite pre-carbon dioxide treatment, while no apparent trace of muscovite post treatment. Also, dolomite was present in sample 8 (Dolomitic-Limestone) pre-carbon dioxide treatment, while no trace of dolomite was recorded post carbon dioxide treatment. Mineralogy is based in part on the JADE ® XRD analytical software. Figure 3.31 shows an example of XRD graph for sample 8 (S-8) pre-carbon dioxide treatment.

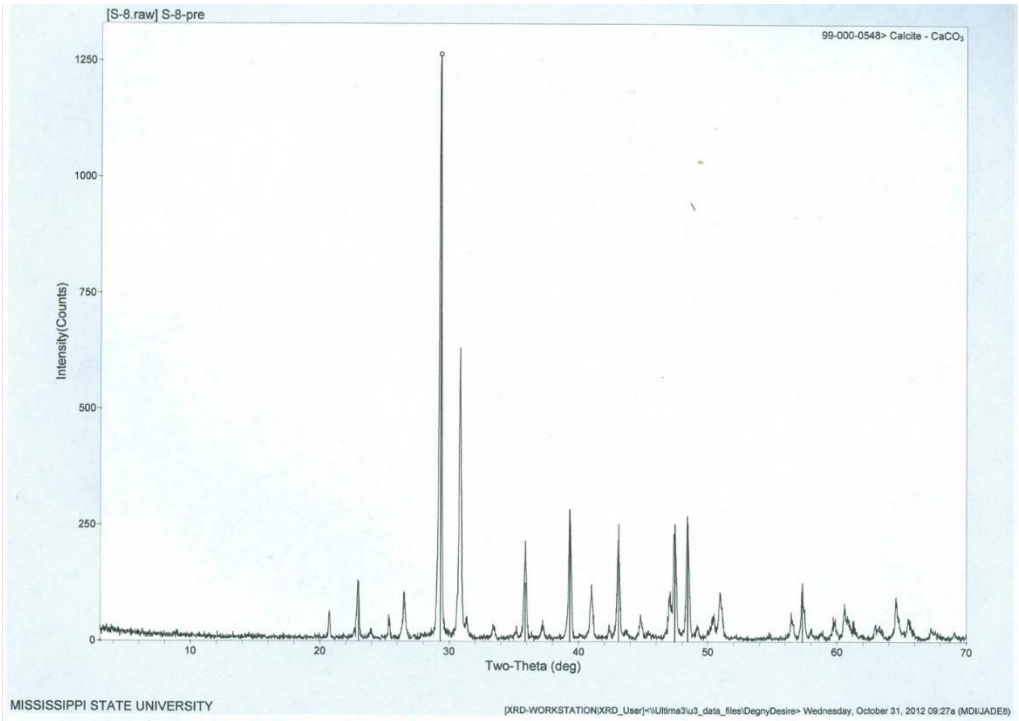

Figure 3.31 XRD shows 29 two-theta (deg) calcite peak in sample 8 (S-8). Also, 31 two- theta (deg) dolomite peak in sample 8.

Table 3.5 Table summarizing XRD results pre- and post-carbon dioxide treatment.

Samples	Lithology	XRD results pre-carbon dioxide	XRD results post-carbon dioxide
St-1	Shaly-sandstone	N/A	Calcite
Sc-2	Limestone (Salem Formation)	Calcite	Calcite
Ssm-3	Sandstone	Quartz	Quartz
Ssm-4	Sandstone	Quartz	Quartz
Se-5	Shaly-Sandstone	Quartz	Quartz
Se-6	Sandstone	Quartz	Quartz
Sun-7	Sandstone	Quartz, Muscovite	Quartz
S-8	Partially dolomitized Limestone (Samckover Formation)	Calcite, Dolomite	Calcite

3.5 Scanning Electron Microscopy (SEM) Results

SEM analysis was conducted for each of the sample with the intent to determine any changes before and after carbon dioxide treatment. SEM enables the study of the microstructure, the micropores, fractures, and the nature of the different minerals present pre- and post-carbon dioxide treatment of the samples.

3.5.1 Sample 1- St-1- Heidelberg field/4,916-5,581 ft

SEM analysis of sample 1 (St-1) pre-carbon dioxide exposure is illustrated in Figure 3.32 showing enlarged fracture in a clay matrix and evidence of clay minerals presence, possibly smectite in Figure 3.33. Post-carbon dioxide analysis of sample 1 revealed possible trace of dissolution and corrosion. Dissolution exhibits karst like structure that could easily be interpreted as pock marks. Corrosion was observed on surface of smectite and surrounding area. Smectite grain shows strong discolorations pattern. Area affected exhibits a strong dark grey coloration compare to unaffected area showing a light grey coloration. Figure 3.34 shows possible dissolution in calcite and what was label as corrosion in smectite in Figure 3.35 post-carbon dioxide treatment.

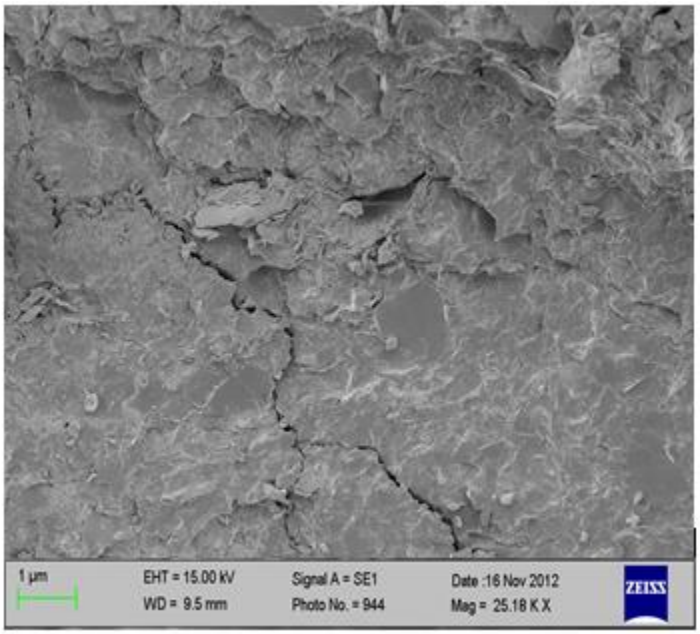

Figure 3.32 St-1- Heidelberg field/4,916-5,581 ft SEM picture shows enlarged fracture in very fine clay matrix. Note flaky aspect of matrix (pre-carbon dioxide).

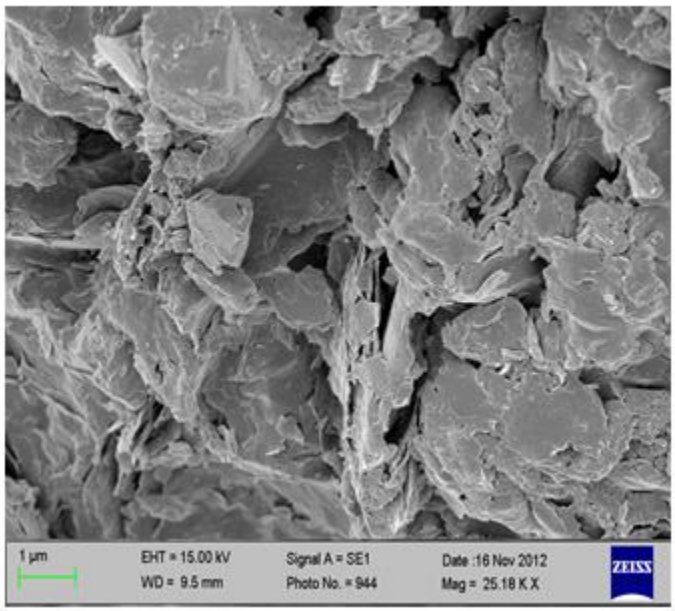

Figure 3.33 St-1- Heidelberg field/4,916-5,581 ft Evidence of clay minerals presence, possibly Smectite (pre-carbon dioxide).

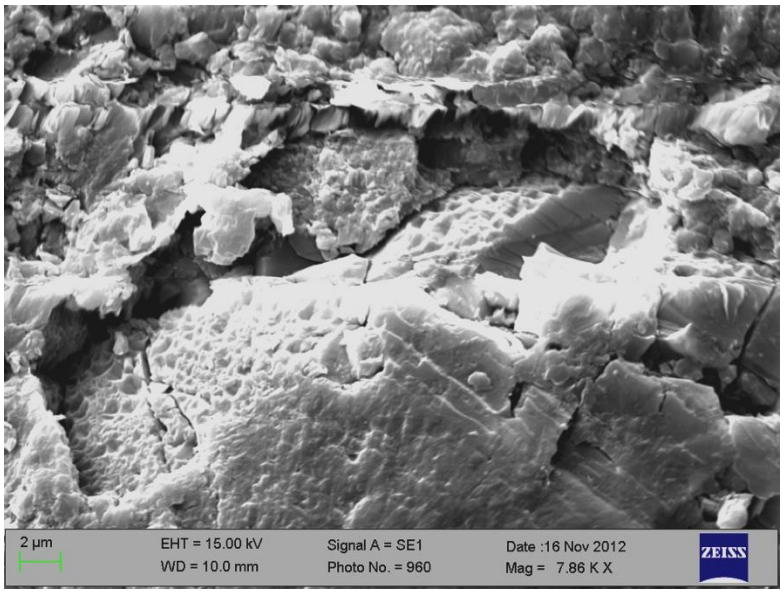

Figure 3.34 St-1- Heidelberg field/4,916-5,581 ft SEM image shows cavity in calcite embedded in clay matrix. Cavity exhibits karst-like structure more like pock marks (post-carbon dioxide).

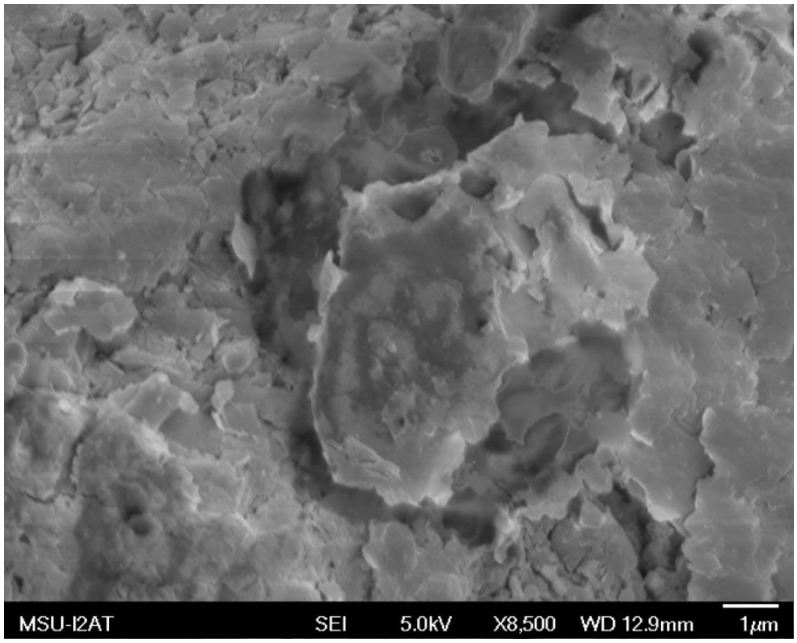

Figure 3.35 St-1- Heidelberg field/4,916-5,581 ft SEM image shows what is believed to be corrosion in smectite grain. Strong discoloration of grain can be noted. The area affected presents a dark grey coloration comparing to the light grey of unaffected area (post-carbon dioxide).

3.5.2 Sample 2- Sc-2- Limestone- Salem Formation (control)

Pre-carbon analysis of sample 2 (Sc-2) is illustrated in Figure 3.36 showing calcite grain exhibiting truncated like shape. The calcite grains are embedded in a micrite matrix and did not show any evidence of dissolution. Figure 3.37 shows interlocking calcite crystals with microporosity and either incomplete crystal growth or dissolution pre carbon dioxide treatment.

Post-carbon dioxide analysis of sample Sc-2 unveiled evidence of dissolution that resembles karst-like features. The dissolution features were only observable at high magnification on calcite crystal surfaces. Figure 3.38 shows possible evidence of dissolution and Figure 3.39 shows dissolution features exhibiting karst-like structures in Sc-2 post carbon dioxide.

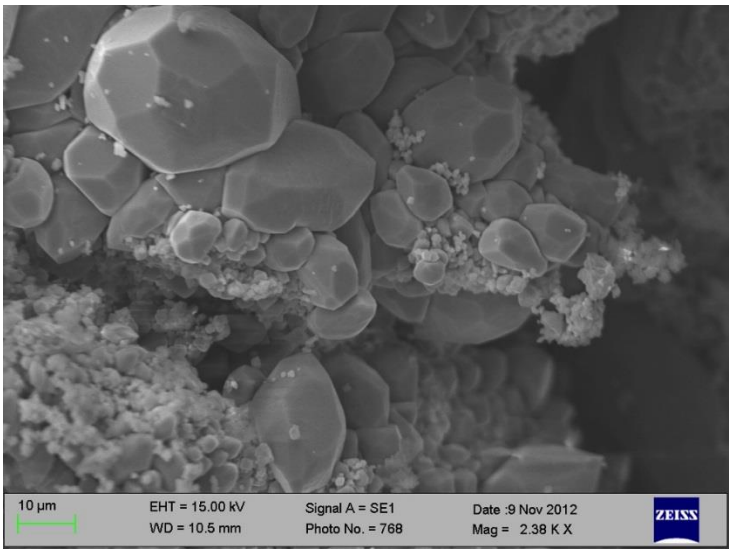

Figure 3.36 Sc-2- Salem Formation (control) SEM image shows calcite grain showing truncated-tetrahedron like shape embedded in a micrite matrix, no evidence of dissolution was observed. Also, calcite crystals have relatively smooth surfaces (pre-carbon dioxide).

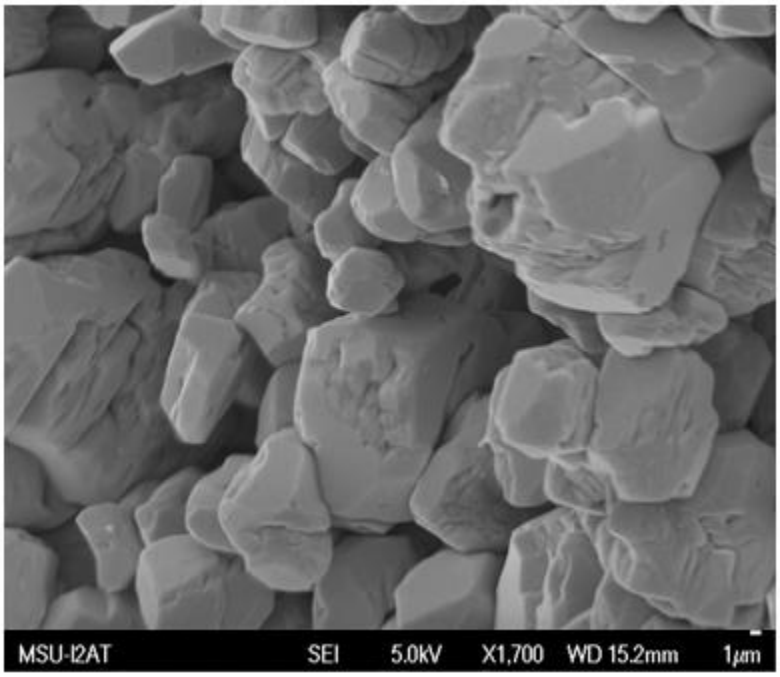

Figure 3.37 Sc-2- Salem formation (control) SEM image shows interlocking calcite crystals with microporosity and either incomplete crystal growth or dissolution (pre-carbon dioxide).

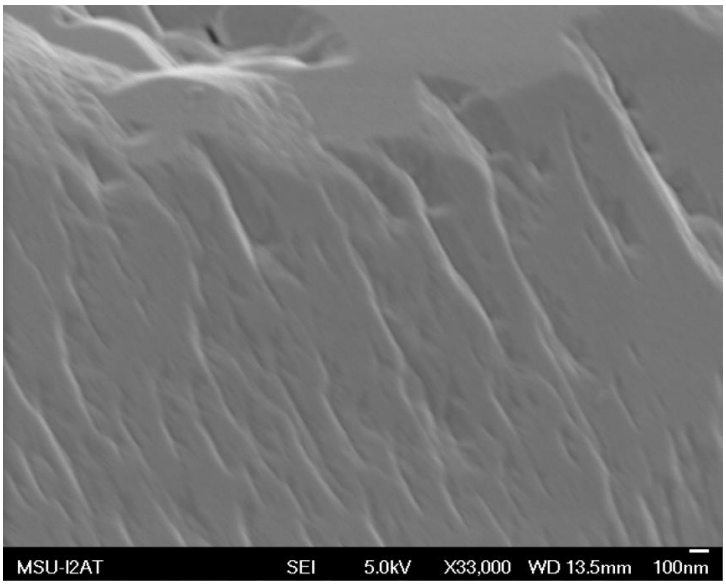

Figure 3.38 Sc-2- Salem Formation (control) High magnification of calcite crystal face showing some possible evidence of dissolution (post-carbon dioxide).

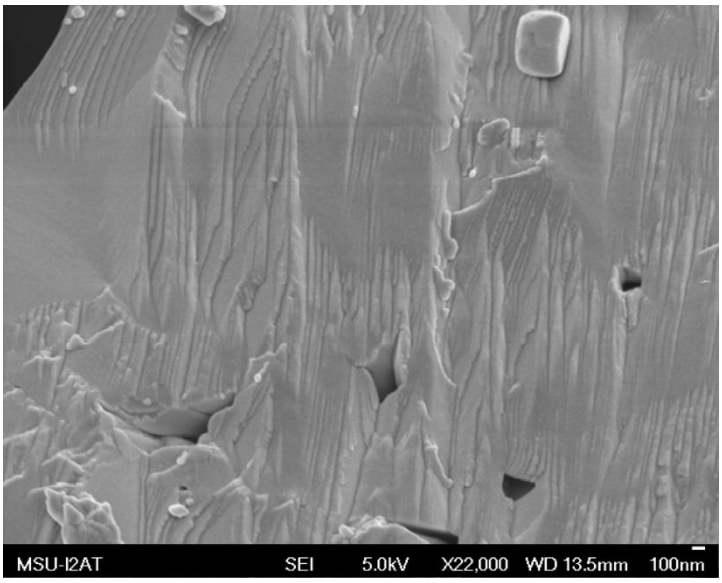

Figure 3.39 Sc-2- Salem formation (control) SEM image shows evidence of dissolution that resembles karst-like features, but at a very small scale (post-carbon dioxide).

3.5.3 Sample 3- Ssm-3- Sandstone-Heidelberg field- 15,231-15,246 ft

Sample 3 (Ssm-3) analysis in SEM shows the presence of clay matrix and quartz grain. Quartz crystals, even though altered, show hexagonal shape. Clay matrix was identified by the flaky-like structure exhibited by most clay minerals. Presence of pores was not recorded but microfracture was observed. Variations in Ssm-3 post-carbon dioxide include abundance of micropores in clay. The micropores present seem to represent dissolution induced by carbon dioxide. Figure 3.40 illustrates quartz grain embedded in clay matrix and partially recovered by clay minerals pre-carbon dioxide. Figure 3.41 shows sparsely distributed micropores in clay. Figure 3.42 shows also micropores in clay.

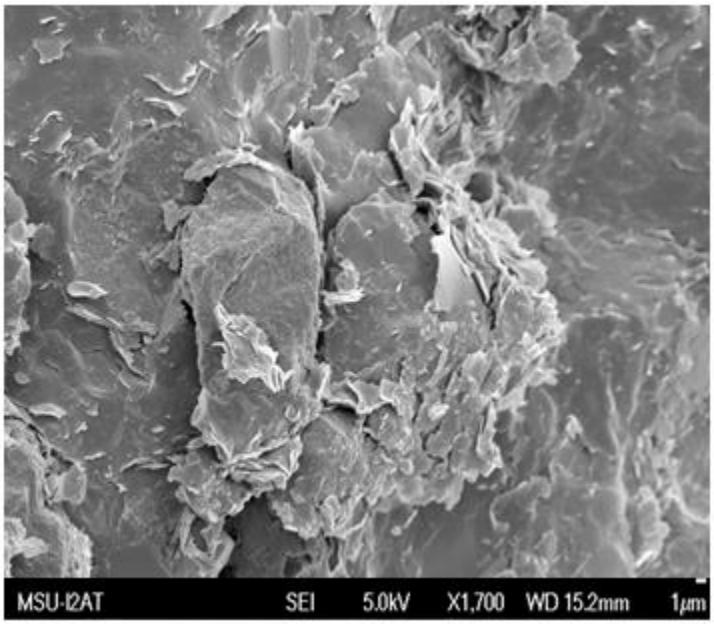

Figure 3.40 Ssm-3- Heidelberg field- 15,231-15,246 ft SEM image shows quartz embedded and partially covered by clay (pre-carbon dioxide).

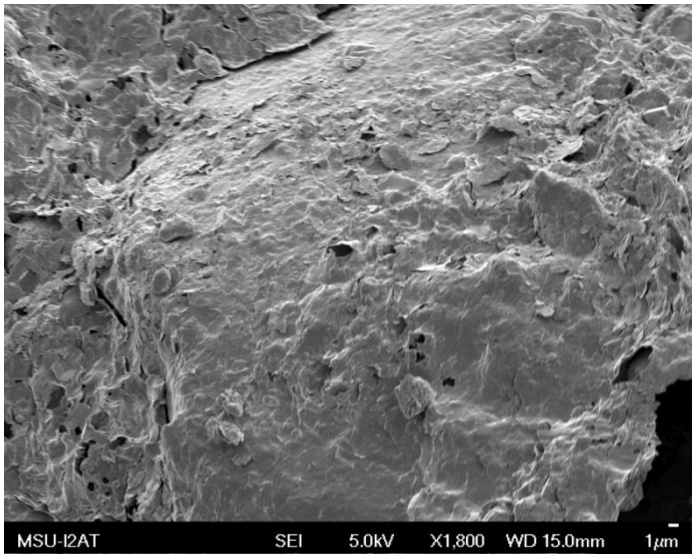

Figure 3.41 Ssm-3- Heidelberg field- 15,231-15,246 ft SEM image shows micropores (post-carbon dioxide).

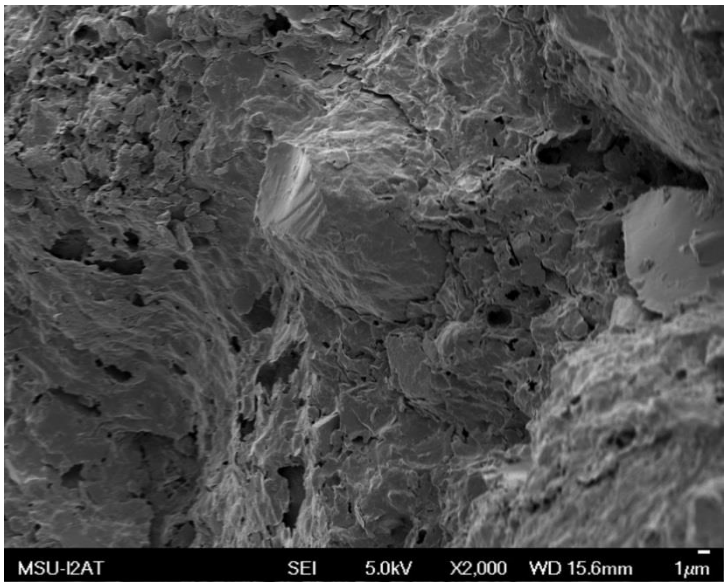

Figure 3.42 Ssm-3- Heidelberg field- 15,231-15,246 ft Higher magnification image of micropores (post-carbon dioxide).

3.5.4 Sample 4- Ssm-4- Sandstone- Heidelberg field- 15,281-15,286 ft

Figure 3.43 shows the presence of altered hexagonal quartz grain embedded in clay matrix, also, microfracture can be observed pre-carbon dioxide treatment. Variation within sample 3 (Ssm-4) post carbon dioxide treatments was not recorded. Post-carbon dioxide analysis revealed the presence of quartz grain embedded in clay matrix. Clay presents flaky structure. Figure 3.44 shows edge of quartz grain embedded in clay matrix and clay mineral exhibiting flaky structure post carbon dioxide.

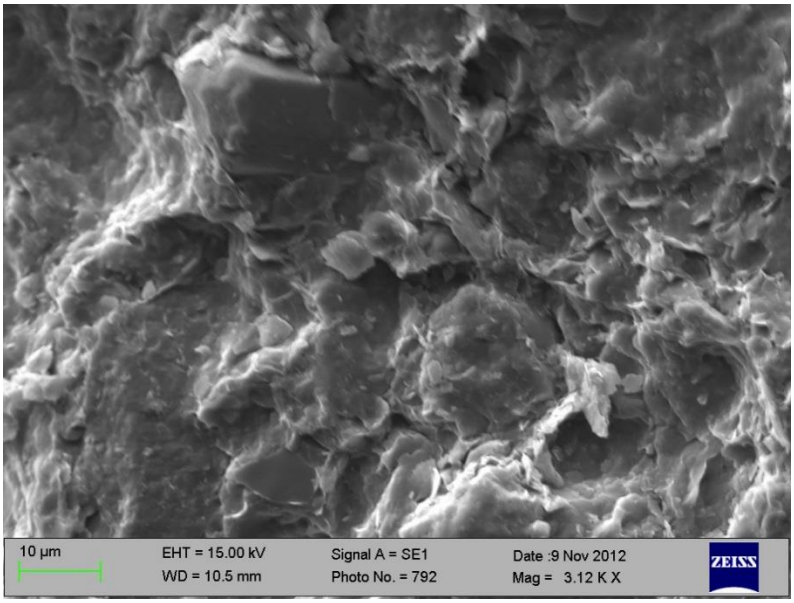

Figure 3.43 Ssm-4- Heidelberg field- 15,281-15,286 ft SEM image shows altered hexagonal quartz grain (top left corner) embedded in clay matrix and microfracture (pre-carbon dioxide).

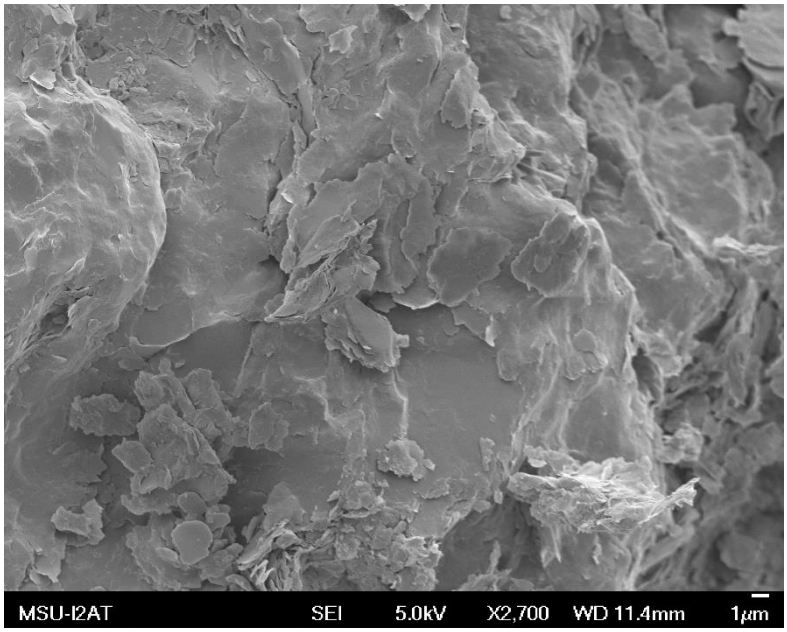

Figure 3.44 Ssm-4- Heidelberg field- 15,281-15,286 ft Picture shows edge of quartz grain embedded in clay matrix and clay mineral exhibiting flaky structure (post carbon dioxide).

3.5.5 Sample 5- Se5- Shaly-sandstone- Heidelberg field- 4,774.5' ft

Sample 5 (Se-5) analyses, pre carbon dioxide, provided evidence of quartz crystals embedded in clay matrix, and possible pyrite in Figure 3.45. Quartz crystals were well developed and showed no evidence of alteration. The crystal size varies from 2 to 1 mm. clay minerals present are mostly kaolinite and seem to fill some of the pores present, however, some voids could be seen in Figure 3.46. Post-carbon dioxide treatment of sample 5 (Se-5) lead to unveiled precipitation of new mineral. The mineral seemed to have precipitated on top of quartz crystals and clay minerals. The mineral exhibits lath shape like structure or band like structure. The new minerals have a size ranging from 1 to 2 mm in length and 0.5 mm in width. Crystals show S, O, and Ca in EDS. Figure 3.47, 3.48, 3.49, and Figure 3.50 illustrated new precipitated mineral in sample 5 (Se-5) and was identified as possible "gypsum".

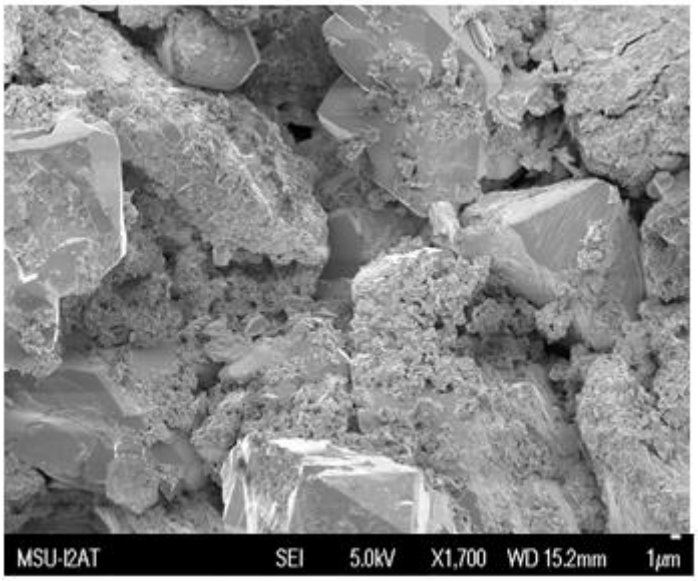

Figure 3.45 Se5- Heidelberg field- 4,774.5’ ft SEM image shows quartz crystals in clay matrix and microporosity (pre-carbon dioxide).

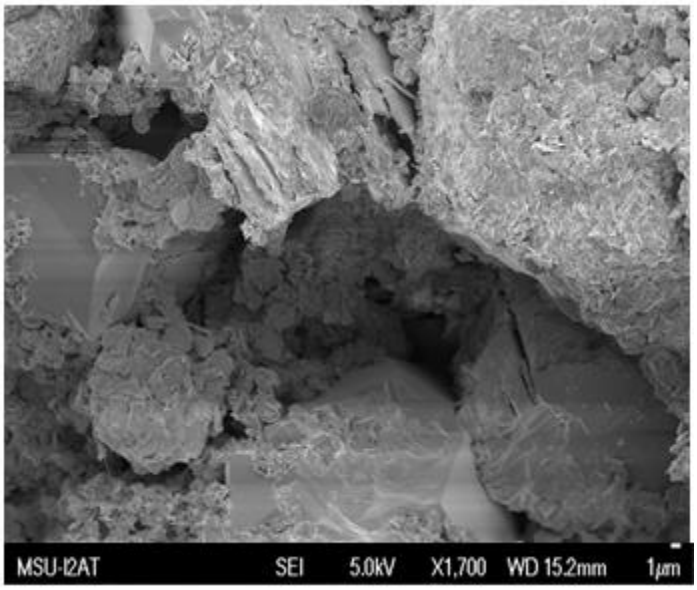

Figure 3.46 Se5- Heidelberg field- 4,774.5' ft SEM image shows quartz crystal over lain by clays minerals, but multiple voids exist (pre-carbon dioxide).

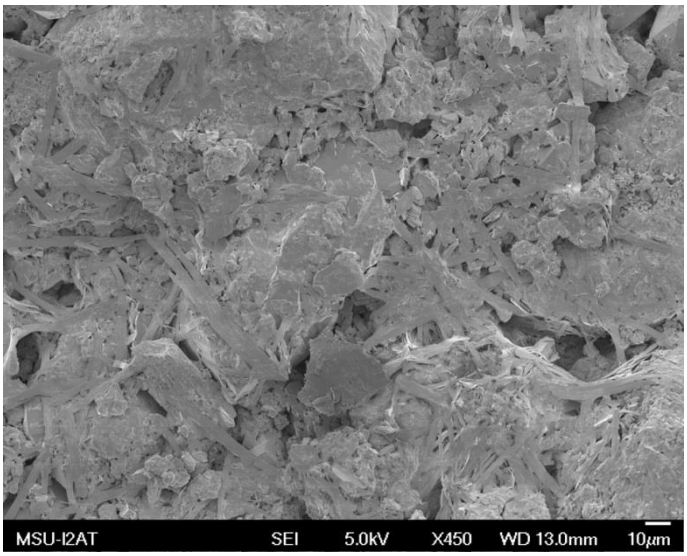

Figure 3.47 Se5- Heidelberg field- 4,774.5' ft SEM image shows precipitation of gypsum in lath shaped crystals. Crystals show S, O, and Ca in EDS (post-carbon dioxide treatment).

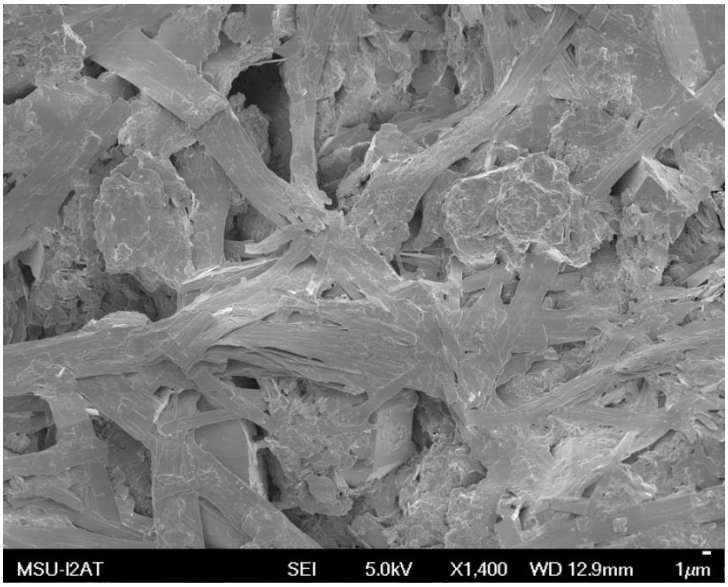

Figure 3.48 Se5- Heidelberg field- 4,774.5' ft High magnification of "gypsum" covering quartz crystals (post-carbon dioxide).

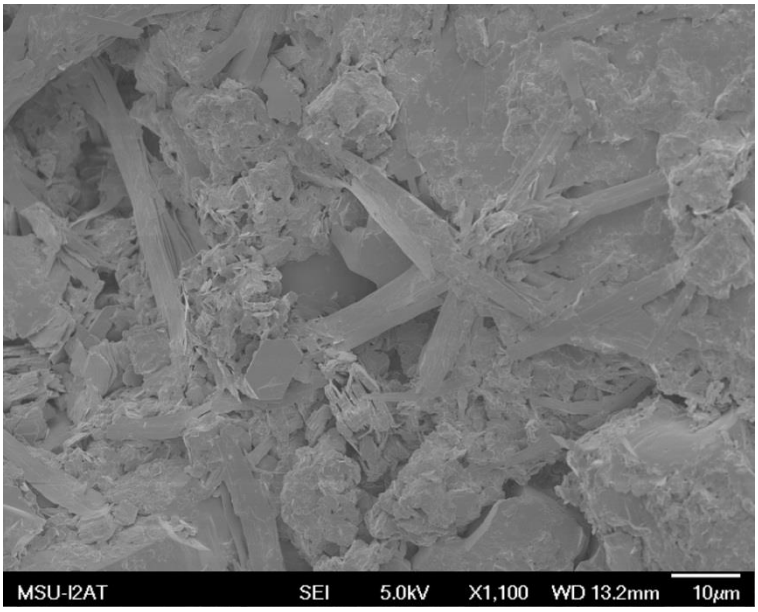

Figure 3.49 Se5- Heidelberg field- 4,774.5' ft SEM image shows flower-like structure growth pattern exhibited by "gypsum" (post-carbon dioxide).

Figure 3.50 Se5- Heidelberg field- 4774.5' ft SEM image shows fiber-like structure of "gypsum" partially occluding pores (post-carbon dioxide).

3.5.6 Sample 6- Se-6- Sandstone- Heidelberg field- 4,709' ft

SEM analysis pre- and post-carbon analysis did not show any variations or changes in sample 6 (Se-6). Figure 3.51 shows larger crystal faces over lain by clays minerals, but multiple voids exist before carbon dioxide exposure. Figure 3.52 shows enlarged fracture in clay matrix post-carbon dioxide.

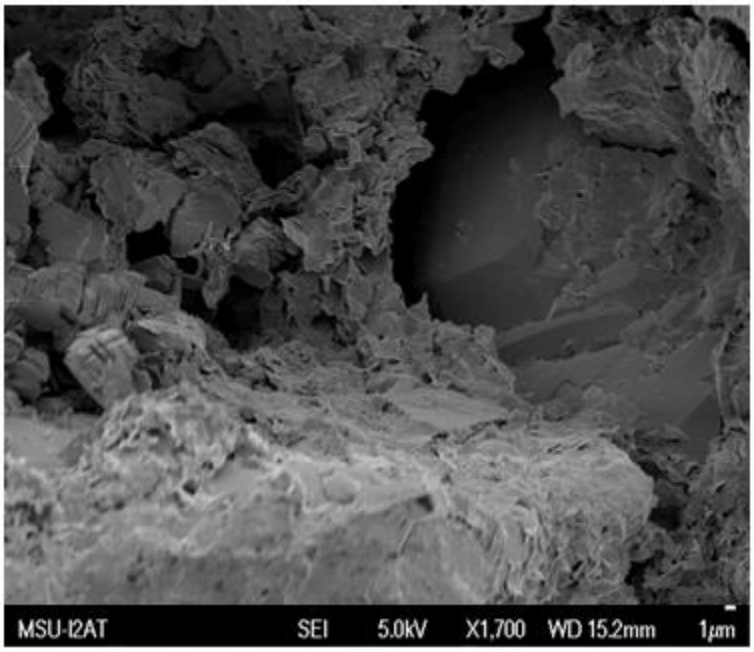

Figure 3.51 Se-6- Heidelberg field- 4,709' ft SEM image shows larger crystal faces over lain by clay minerals, but multiple voids exist (pre-carbon dioxide).

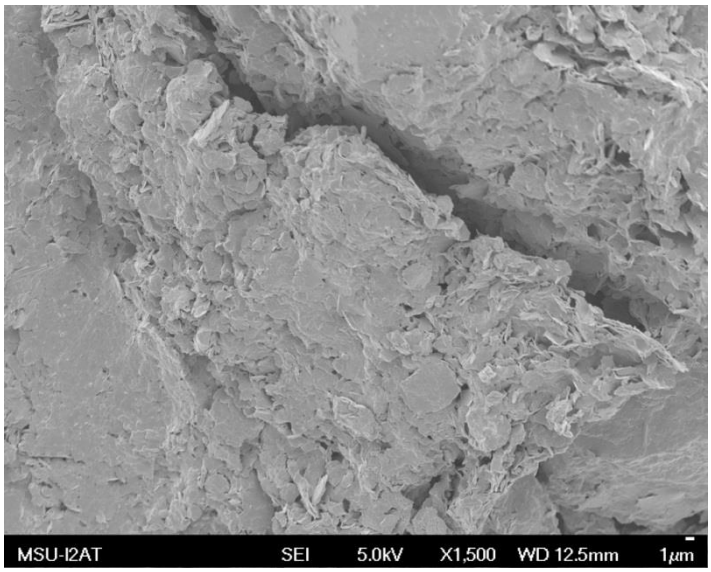

Figure 3.52 Se-6- Heidelberg field- 4,709' ft SEM image shows enlarged fracture (post-carbon dioxide).

3.5.7 Sample 7- Sun-7- Sandstone- Heidelberg field- 8,410-8,787' ft

SEM Pre-carbon analysis of sample 7 (Sun-7) is illustrated in Figure 3.53 showing well developed quartz crystal embedded in clay matrix. Figure 3.54 shows conglomeration of possible clay minerals in cluster post-carbon dioxide.

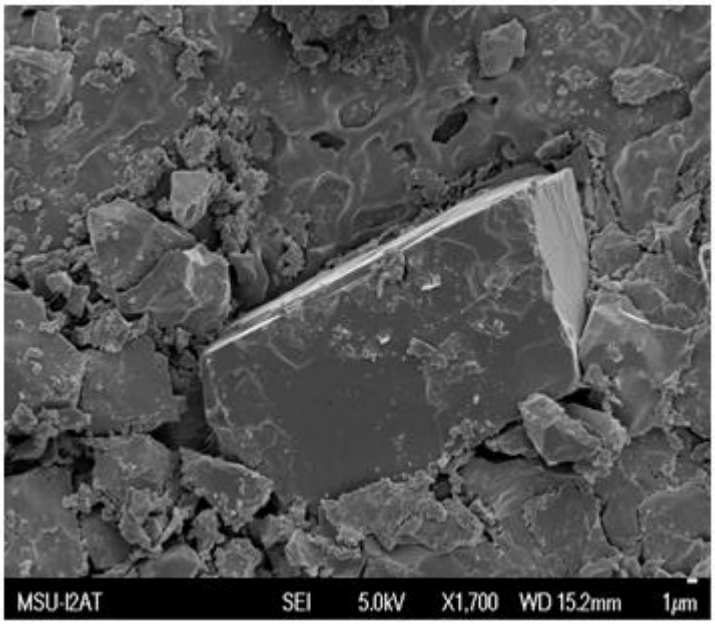

Figure 3.53 Sun-7- Heidelberg field- 8,410-8,787' ft SEM image shows well developed quartz crystal embedded in clay matrix (pre-carbon dioxide).

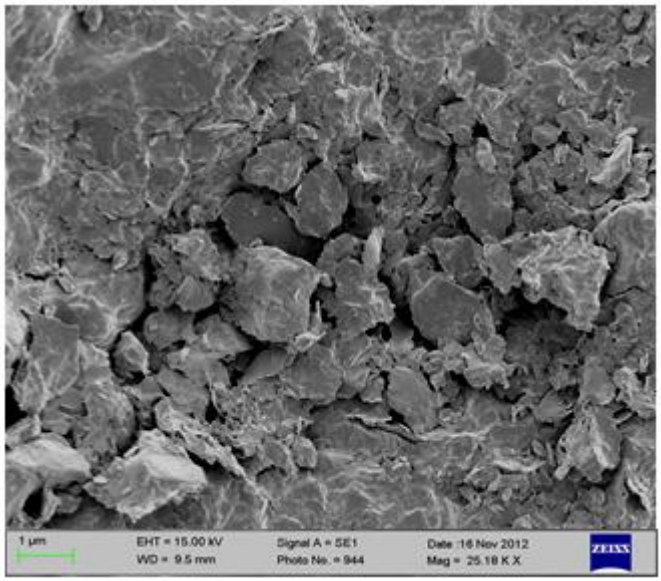

Figure 3.54 Sun-7- Heidelberg field- 8,410-8,787' ft SEM image shows conglomeration of possible clay minerals in a cluster. Also, Note significant inter particle porosity between grains and flakes of clay (post-carbon dioxide).

3.5.8 Sample 8- S-8- Dolomitic-Limestone- Smackover core

Sample 8 (S-8) represents the Smackover formation. SEM analysis illustrated the presence of well developed dolomite crystal embedded in micron size calcite. Crystal faces are very smooth and present no apparent alteration. Calcite minerals were also observed and presented evidence of alteration. Abundance of microporosity and microfracture were recorded. Exposure of sample to carbon dioxide engendered precipitation of a new mineral on the surface. The new mineral exhibits a flower like structure. The mineral seemed to have grown from a central point and branched out. Flowers sizes are roughly 0.50 to 0.25 mm. Crystals show O, Ca, S, and Mg in EDS. Figure 3.55 shows partially altered calcite embedded in micro size calcite and Figure 3.56 shows image of rhombohedral dolomite within micron size calcite crystals prior to

treatment with carbon dioxide. Figure 3.57, 3.58, 3.59 shows gypsum mineral exhibiting flower like structure.

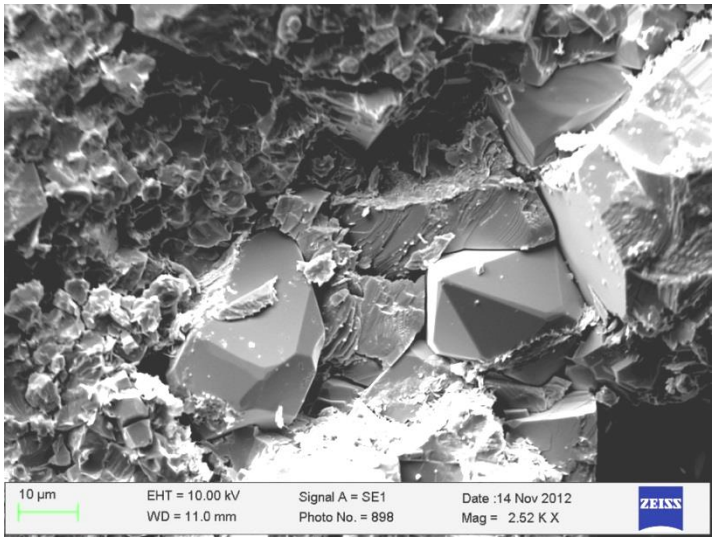

Figure 3.55 S-8-Smackover core SEM images of partially altered calcite crystals and microfractures (pre-carbon dioxide).

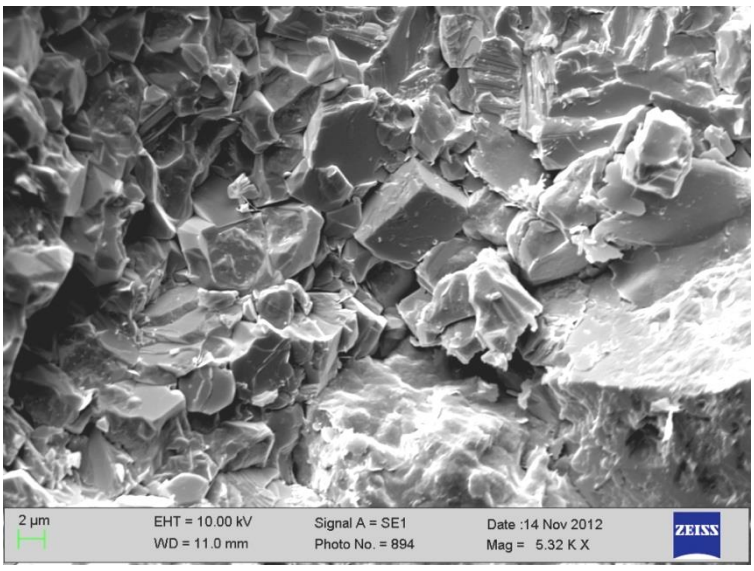

Figure 3.56 S-8-Smackover core SEM image of rhombohedral dolomite within micron size calcite crystals and open microporosity (pre-carbon dioxide).

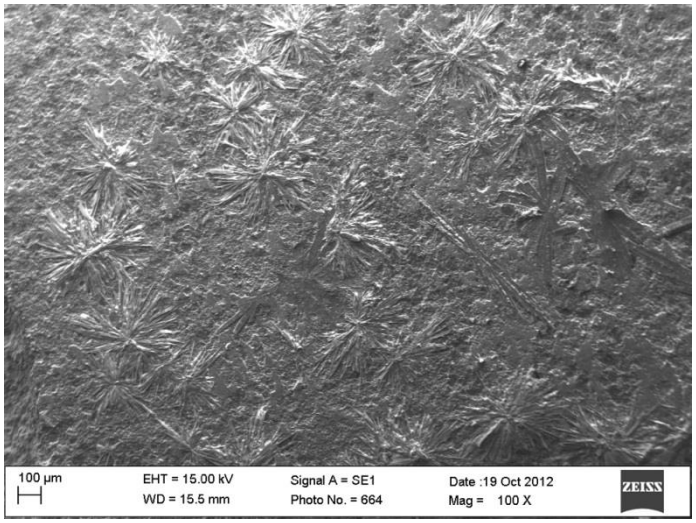

Figure 3.57 S-8-Smackover core SEM image shows flower like structure of newly precipitated "gypsum" (post-carbon dioxide).

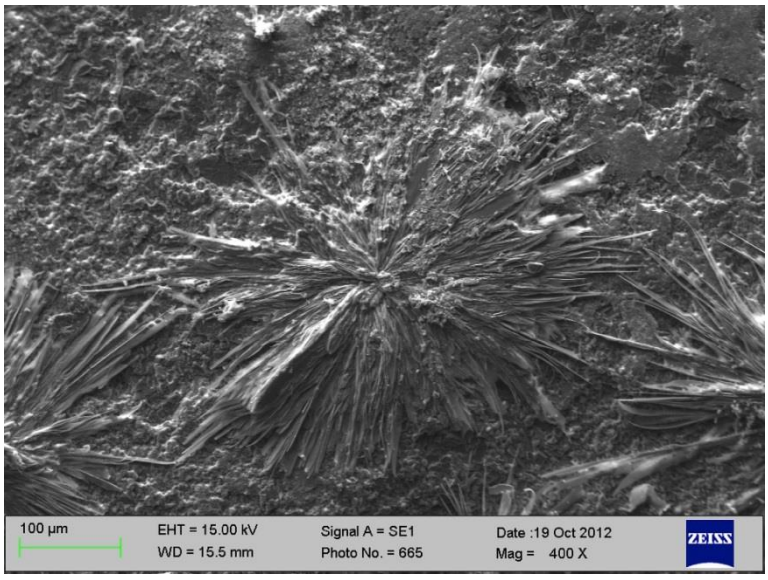

Figure 3.58 S-8-Smackover core High magnification images of gypsum "flowers" (post-carbon dioxide).

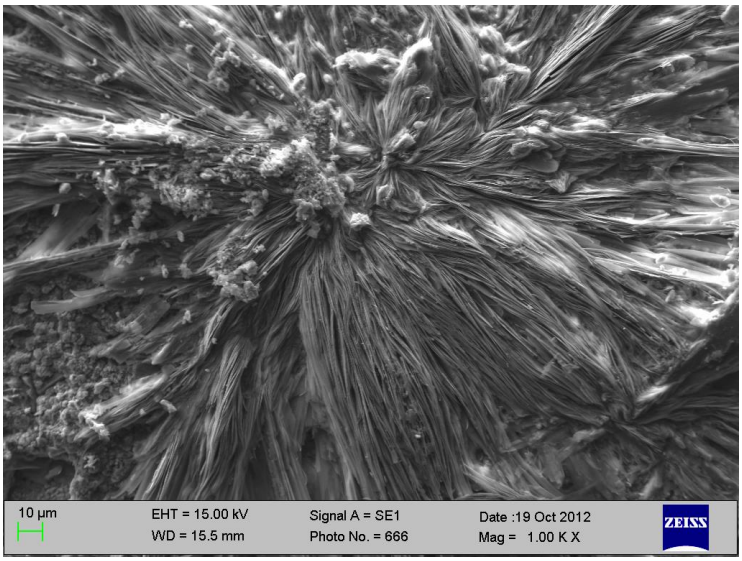

Figure 3.59 S-8-Smackover core SEM image shows possible point of growth start of "gypsum" (post-carbon dioxide).

3.6 EDS Results

EDS analysis was performed on sample Se5 (Shaly-sandstone) and S-8 (Dolomitic-Limestone) post carbon dioxide to determine the nature of the elements from the possible precipitation of new minerals, which one was interpreted as gypsum. In sample Se-5, the gypsum presents a lath or fibrous like structure while in sample S-8 it exhibits a flower like structure. Also, strong evidence of Oxygen (O), Sulfur (S), Magnesium (O), and Calcium (Ca) can be recorded in the area covered by the gypsum. Figure 3.60 represents EDS analysis for Se-5 and Figure 3.61 shows elemental mapping for SE-5. Figure 3.62 shows EDS analysis for S-8 and Figure 3.63 shows elemental mapping for S-8. All EDS analyses and elemental mapping were conducted post-carbon dioxide treatment.

3.6.1 Sample 5 – Se-5 – Shaly-sandstone- 4,774.5 ft (Heidelberg Field)

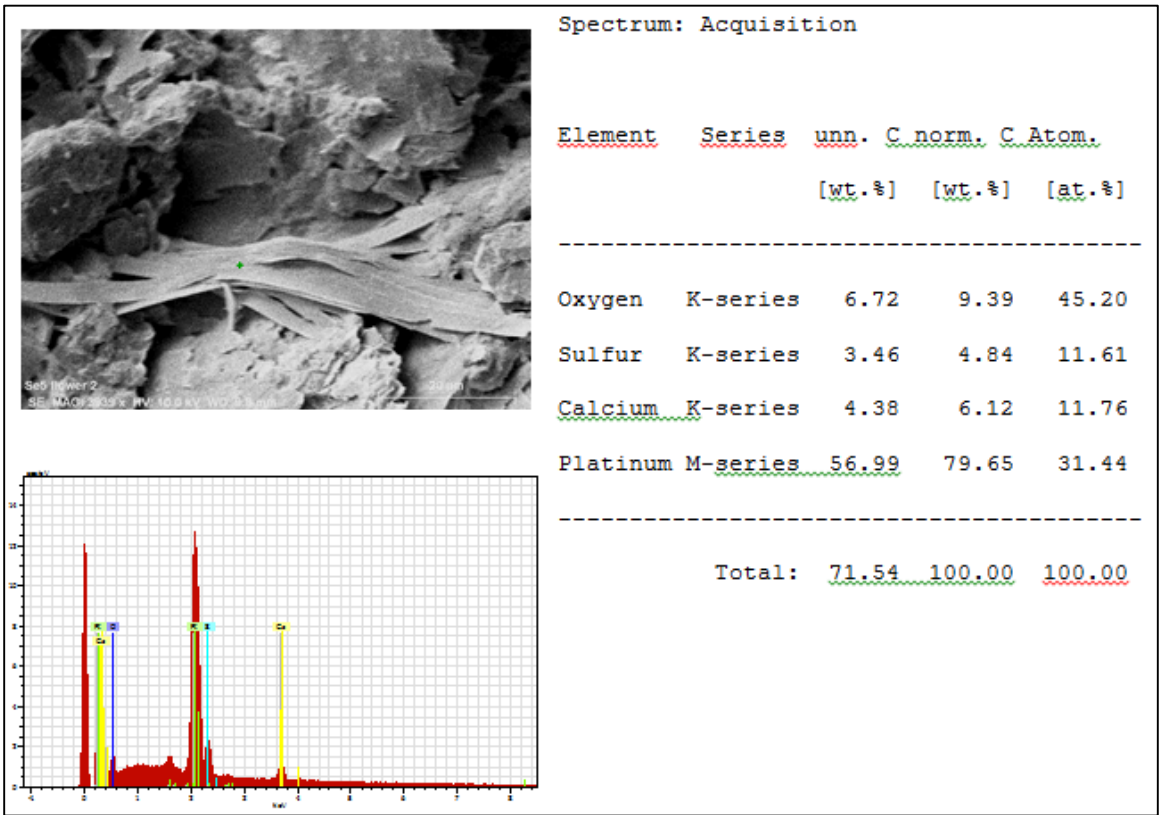

Spectrum: Acquisition

Element	Series	unn. C [wt.%]	norm. C [wt.%]	Atom. C [at.%]
Oxygen	K-series	6.72	9.39	45.20
Sulfur	K-series	3.46	4.84	11.61
Calcium	K-series	4.38	6.12	11.76
Platinum	M-series	56.99	79.65	31.44
Total:		71.54	100.00	100.00

Figure 3.60 FESEM Se-5. 4,774.5 ft EDS analysis shows elements of mineral occurring post carbon dioxide treatment. New mineral seems to have precipitated on top of clays. Elements found include oxygen (O), calcium (Ca), sulfur (S), and platinum (Pt). All samples were coated with platinum, explaining the platinum peaks.

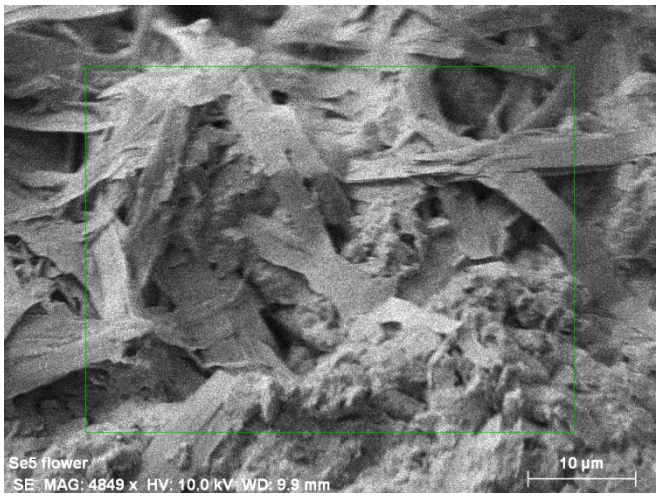

Figure 3.61 FESEM Se-5 (Heidelberg Field)/4,774.5 ft Gypsum lath seems to have precipitated on top of clays after carbon dioxide treatment.

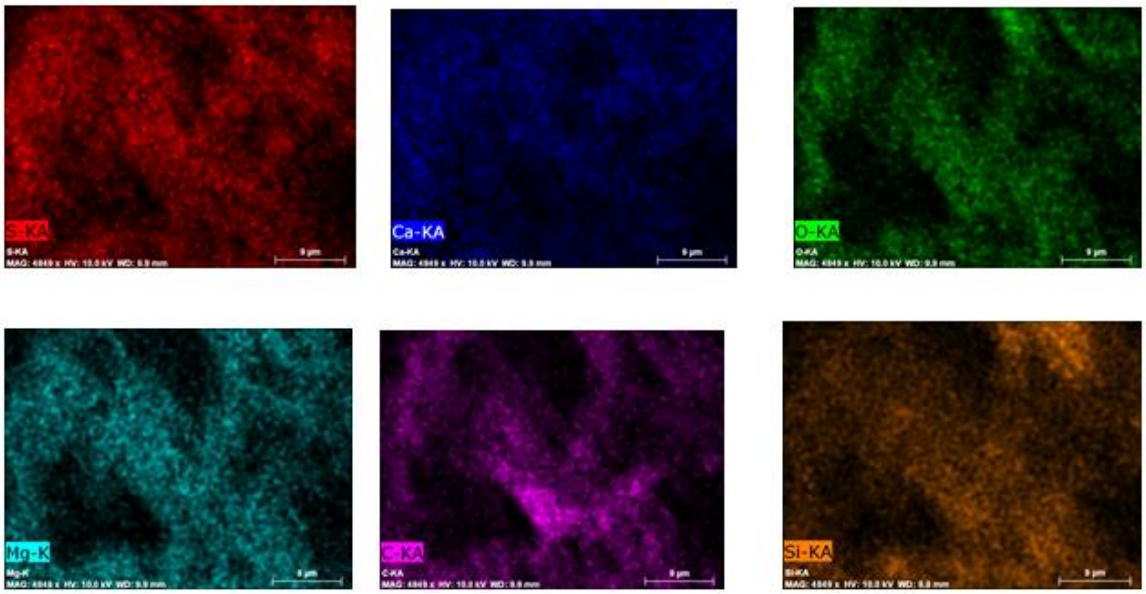

Figure 3.62 Se-5 (Heidelberg field)/4,774.5 ft Elemental mapping of gypsum lath occurring on top of clays post-carbon dioxide treatment. Note strong evidence of sulfur (S), oxygen (O), magnesium (Mg), calcium (Ca) in the area covered by the gypsum lath.

3.6.2 Sample S-8 – Dolomitic-Limestone (Smackover core)

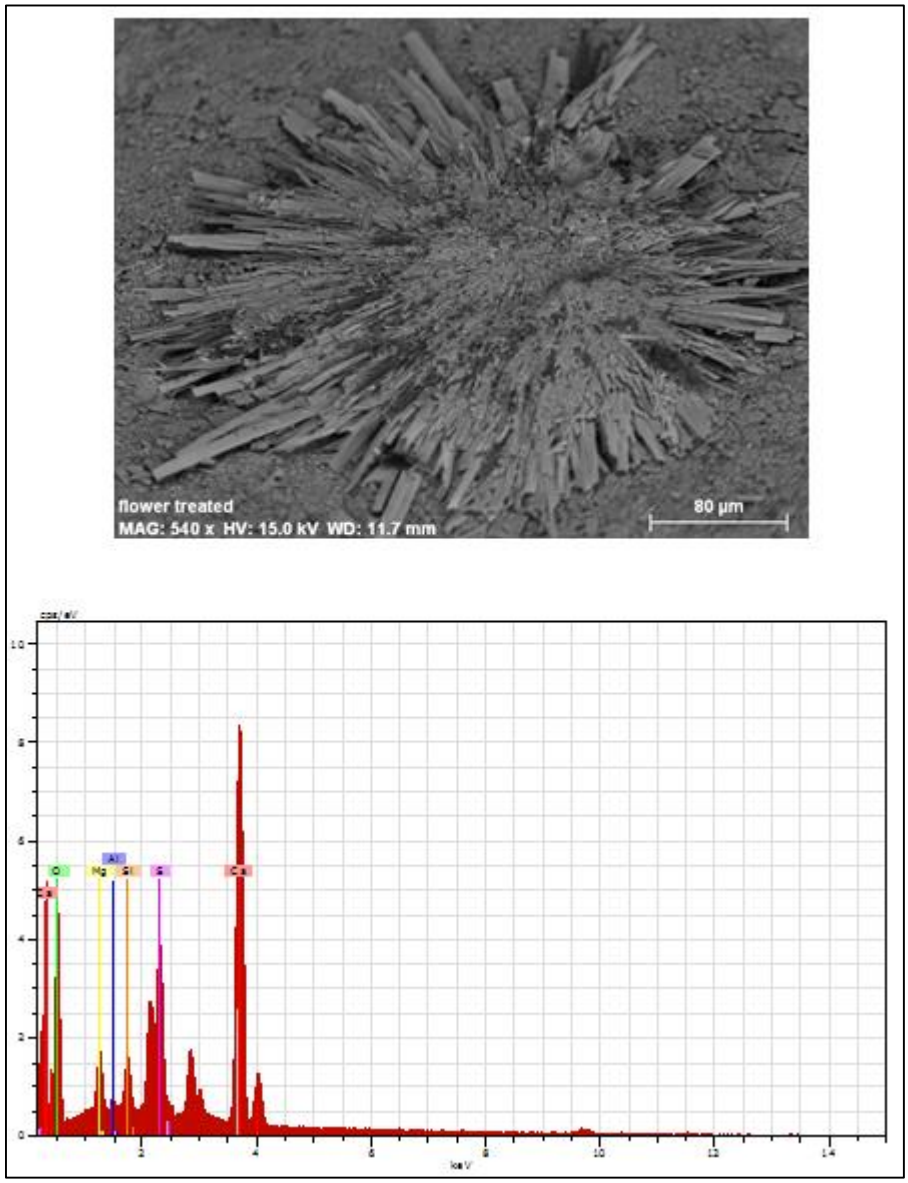

Figure 3.63 FESEM S-8 Smackover core EDS analysis shows elements in the newly precipitated mineral. Elements present are calcium (Ca), magnesium (Mg), oxygen (O), and sulfur (S).

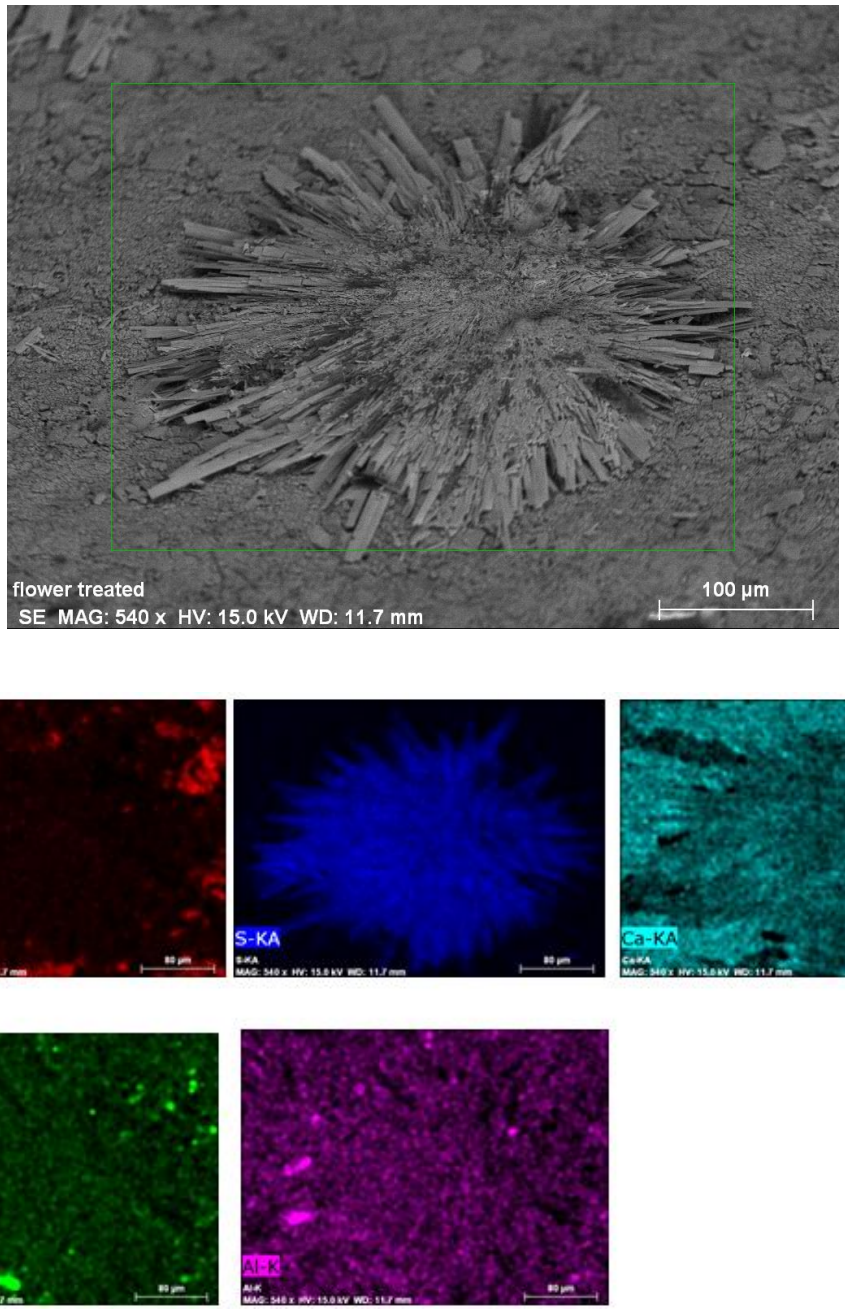

Figure 3.64 S-8 Smackover core Elemental mapping of gypsum flower provided evidence of sulfur (S), magnesium (Mg), and calcium (Ca).

3.7 Focused Ion Beam Tomography-SEM Results

FIB-SEM analysis was conducted to understand the microstructure of sample eight (dolomitic-limestone) pre and post carbon dioxide. Pre carbon dioxide FIB results show the distribution and arrangement of the pore system, the type of pores, and their connectivity relative to each other. Figure 3.65 represents a single image generated using FIB. A series of image were generated and a 3D reconstruction of the microstructure of the area studied was developed and showed in Figure 3.66. Post-carbon dioxide analysis provided the distribution of the gypsum minerals. Gypsum seemed to have precipitated in some of the pores and occluded porosity, thus reducing permeability of the sample. Figure 3.67 illustrates a single image generated post carbon dioxide using FIB.

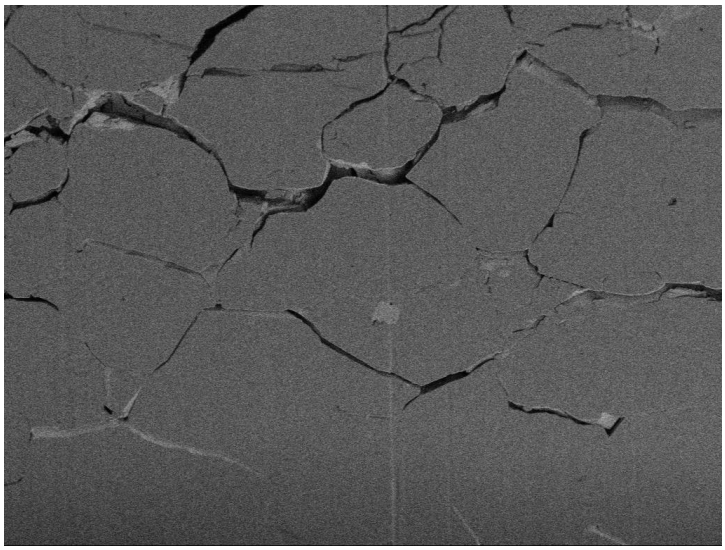

Figure 3.65 FIB-S-8 (dolomitic-limestone)/Smackover Fm Image showing a cross section generated by FIB. Note pores on image surface (pre-carbon dioxide).

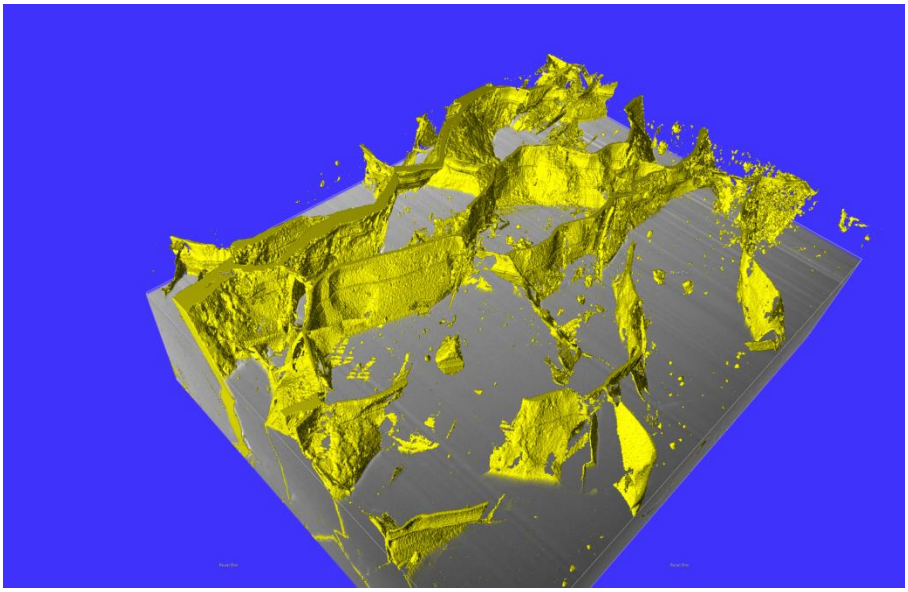

Figure 3.66 FIB-S-8 (Dolomitic-limestone)/Smackover Fm Image shows 3D reconstruction of sample 8 pore system and connectivity (yellow), using the different pictures generated by FIB pre-carbon dioxide.

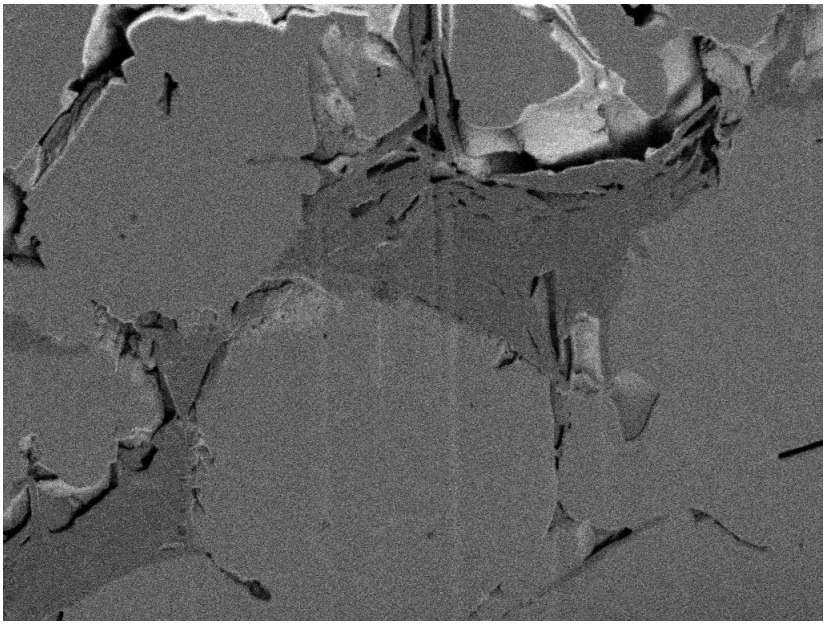

Figure 3.67 FIB- S-8 (dolomitic-limestone)/Smackover Fm Image of 1 cross section of sample 8 post-carbon dioxide.

Pores seem to be filled with new elements (post-carbon dioxide).

CHAPTER IV

DISCUSSION

Carbon dioxide is one of the most significant emitted anthropogenic gases in the atmosphere in this century ([IPCC], 2005). Reducing the emission of carbon dioxide has been one of the biggest challenges not only for the energy industry but also for environmentalists. Many studies have proven that CO_2 storage and sequestration in geologic formations or use in EOR are potential options to considerably reduce the impact of carbon dioxide without impacting our daily production and use of energy. However, geologic formations, due to different lithologies, will chemically react with the carbon dioxide upon storage and sequestration. This study has attempted to determine the different and possible impacts generated by carbon dioxide on different lithologies, specifically those found in the Heidelberg field, south central Mississippi.

Thin section analyses of pre- and post- carbon dioxide impact on siliciclastic and carbonate rocks has revealed strong evidence of alteration in three samples: 1) sample 1-St-1 (Heidelberg field/ 4,916-5,581 ft) obtained from the Heidelberg field and characterized by quartz grains and calcitic shells of gastropod embedded in a calcite matrix, 2) sample 2 (carbonate/limestone) associated with the Salem Formation and described as a carbonate, 3) Sample 5 (shaly-sandstone/ 4,774.5’ ft) is from the Heidelberg field and made up of tightly packed sand grains dominated by quartz grains with remaining minerals being muscovite, glauconite, and possibly siderite. The different

alterations recorded in thin sections were mostly dissolution in calcite minerals and precipitation of unidentifiable elements. In sample St-1 dissolution mainly occurred in calcitic gastropod shell (Figure 3.7 and 3.8), in sample Sc-2 (carbonate/limestone) dissolution occurred mainly in calcite cement (Figure 3.11). Dissolution in St-1 and Sc-2 seems to be related to the presence of calcite in abundance in both of the samples. These observations are in agreement with the observations of Pearce *et al.* (1996), Rochelle *et al.* (1996), and Gunter *et al.* (1997). During an experiment run for 1 to 8 months involving carbon dioxide, at temperatures of 105º and 80º C, a sandstone rich in calcite and dolomite, subsequent dissolution of calcite and dolomite was observed (Pearce *et al.,* 1996; and Rochelle *et al.,* 1996). Furthermore, in a similar experiment but this time on glauconitic sandstones (Alberta sedimentary basin), at a temperature of 105º C, dissolution of carbonate minerals occurred (Gunter *et al.,* 1997). Calcite and dolomite are two minerals prone to dissolution under specific conditions. The relative high pressure and temperature (80º to 100º C) suggested that carbon dioxide presence led to a decrease in the pH of the system (Emberley *et al.,* 2004, 2005), making the system more acidic, facilitation the dissolution of calcite and dolomite. Although dissolution in St-1 and Sc-2 was favored by the presence of calcite, no apparent dissolution was observed for S-8 (dolomitic-limestone), which is characterized by the abundance of calcite and dolomite. The possible explanation is that even if precipitation occurred, precipitation of "gypsum" may have overprinted traces of dissolution. Precipitation of gypsum could not be fully acknowledged in thin section.

Porosity analyses of the samples before and after carbon dioxide treatment did not unveil any considerable difference. The porosity after carbon dioxide exposure shows similar trends with slight variation in samples St-1 and S-7 (Figure 3.68).

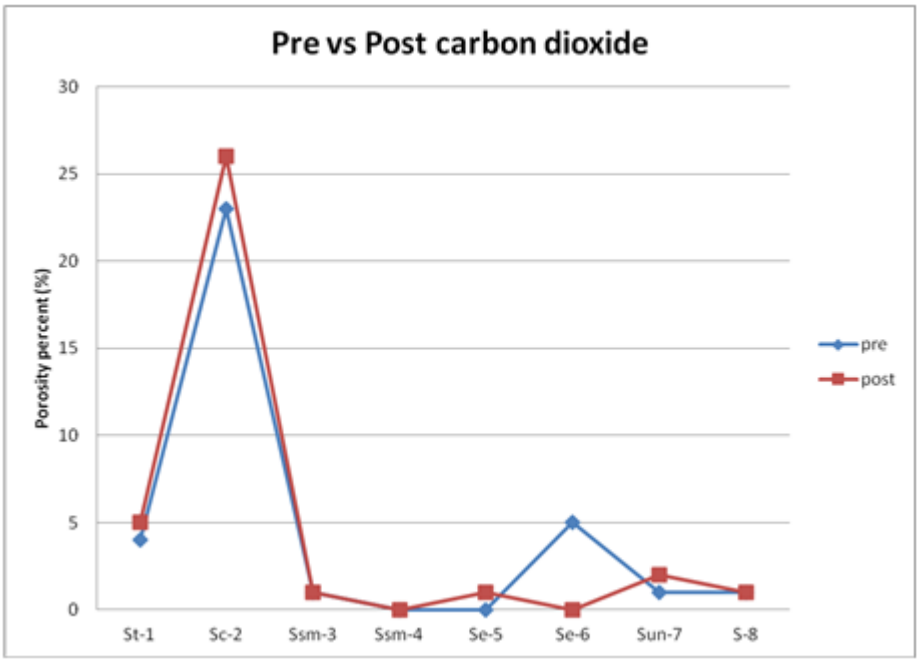

Figure 4.1 Pre vs Post carbon dioxide porosity trend for each of the eight samples. Blue line repesents samples pre-carbon dioxide and red line represents post-carbon dioxide.

The two graphs were generated to compare porosity for each sample before and after exposure to carbon dioxide. The blue line represents the porosity trend for each sample pre- carbon dioxide treatment, while the red line represents post-carbon dioxide treatment porosity trend. The slight or no apparent change recorded in the porosity data after exposure to carbon dioxide was attributed to the possible low rate of dissolution that may have occurred in the samples. Although dissolution occurred, it was probably not

enough to quantitavely record an apparent change between the porosity before and after exposure to carbon dioxide.

SEM analyses revealed not only dissolution, but also precipitation of new mineral respectively in sample St-1 (Heidelberg field/4,916-5,581 ft) in Figure 3.34, sample Sc-2 (carbonate/limestone) in Figure 3.38 and 3.39, and sample Ssm-3 (sandstone/ 15,231-15,246 ft) in figure 3.41 and 3.42, sample Se-5 (shaly-sandstone/ 4,774.5' ft) in Figure 3.47, 3.48, 3.49, and 3.50, and sample S-8 (dolomitic-limestone) in figure 3.56, 3.57, and 3.58. The newly precipitated mineral exhibits lath like structure in sample Se-5 and flower-like structure in sample S-8 (dolomitic-limestone). In sample Se-5 (shaly-sandstone), the new mineral seems to have grown on top of the pre-existing minerals (Figure 3.47, 3.48, 3.49, and 3.50), when in sample S-8 (dolomitic-limestone), it seems that the mineral grew on the surface from a focal point out (Figure 3.57, 3.58, and 3.59). EDS analysis and elemental mapping provided strong evidence that the new mineral contained the following elements: sulfur, oxygen, calcium, and some magnesium; thus, leading to conclude that the mineral is probably gypsum. Gypsum is characterized by tabular, diamond, or fibrous shaped (Pellet, 2002). The chemical formula of gypsum is $CaSO_4.2H_2O$, and consists of strongly bonded layers of SO_4^{2-} and Ca^{2+} with layers of H_2O molecules (Nesse, 2000). The formation of the gypsum in sample Se-5 and S-8 is somewhat unclear, but could be related to the minerals in presence. Sample Se-5 is, a shaly-sandstone from the Heidelberg field, characterized by tightly packed sand grains dominated by quartz grains with remaining minerals being muscovite, glauconite, pyrite, cacite, and possibly siderite. Sample S-8 is, a dolomitize-limestone from the Smackover Formation, characterized by calcite, dolomite, and pyrite. The suggestion for the

formation of gypsum within those samples was tied to the presence of Sulfide mineral (pyrite, FeS_2) and carbonate minerals (calcite, $CaCO_3$; and dolomite, $CaMg(CO_3)_2$). The carbon dioxide, at relative high temperature and pressure, was able not to only oxidized our system but also lower the pH of the system, thus making it more acidic. The decrease of the pH may have induced dissolution of carbonate minerals present (calcite), saturating the system in Ca^{2+}. Also, pyrite oxidation will lead to the productivity of SO_4^{2-} in the system. Once the system was saturated with respect to two elements, reaction occurred between Ca^{2+} and SO_4^{2-} in presence of water, leading to the precipitation of gypsum. A similar mechanism was suggested for the formation of diagenetic gypsum and dolomite in a cold water coral mound in the Porcupine Seabight, off Ireland (Deutsch, 1997; Pirlet *et al.,* 2010). Pyrite oxidation, in a system rich in carbonate minerals, will lead to release of SO_4^{2-} in the system, subsequently increasing the acidity, thus promoting the dissolution of calcite and introduction of Ca^{2+} in the system; thus, upon saturation of SO_4^{2-} and Ca^{2+}, precipitation of gypsum will be recorded (Deutsch, 1997; Pirlet *et al.,* 2010). The following equations show the possible reaction leading to the precipitation of gypsum: equation 4.1 represents only the reaction between calcium and sulphate in presence of water leading to gypsum precipitation, when equation 4.2 represents the total reaction from oxidation of pyrite to gypsum precipitation and by products.

$$2SO_4^2 + 2Ca^{2+} + 4H_2O \rightarrow 2\ CaSO_4.2H_2O \qquad \text{(Eq. 4.1)}$$

(Pirlet et al., 2010)

$$FeS_2 + 15/4\ O_2 + 9/2\ H_2O + 4CaCO_3 \rightarrow 4\ Ca^{2+} + 4\ HCO_3 + 2\ SO_4^{2-} +$$
$$FeOOH + 2\ H_2O \rightarrow 2\ CaSO_4.2H_2O_{(s)} + 2\ Ca^{2+} + 4HCO3 + FeOOH \quad \text{(Eq. 4.2)}$$

(Pirlet *et al.,* 2010)

This study presented some limitations. The first limitation encountered was the slow kinetics of the reactions. Reactions involving carbon dioxide with rocks and minerals tend to occur at a slow rate and require a long time to come to completion (Marini, 2007). Also, the temperature and pressure in the laboratory do not fully represent all field conditions. The experiment was designed to approximate as closely as possible the effects of overburden pressure and geothermal gradient, but was limited by the functional temperature of the oven we had access to in the lab. Further, heterogeneity of some of the samples made it difficult to adequately compare the change in some of the samples. Finally, some of the reactions occurring between carbon dioxide and some of the minerals are very complex. This study is a first look at this complex problem and forms a basis for future, more details studies.

CHAPTER V

CONCLUSIONS

The research performed for this study has resulted in four major conclusions regarding the possible impact of carbon dioxide on different lithologies in the subsurface of south-central Mississippi, specifically from the Heidelberg field:

1. Carbon dioxide has induced alteration in sample St-1 and Sc-2. The alterations recorded were dissolution and corrosion. Dissolution of calcite a replacing gastropod shell was observed in St-1 (Heidelberg field/ 4,916-5,581 ft) and in calcite cement in sample Sc-2 (carbonate/limestone). Dissolution was mostly observed in thin sections. Corrosion in St-1 occurred on possible smectite grain and was observed at SEM.
2. Precipitation of gypsum in sample Se-5 (shaly-sandstone) and S-8 (dolomitic-limestone) was recorded and observed at the SEM. The formation of gypsum is associated with oxidation of pyrite and dissolution of calcite, leading to the release of Ca^{2+} and SO_4^{2-} . Upon saturation of the system, reaction between Ca^{2+} and SO_4^{2-} occurred and led to the precipitation of gypsum ($CaSO_4 \cdot 2H_2O$). Carbon dioxide and high temperature promote reaction in the system.
3. Qualitatively, porosity in sample St-1 (Heidelberg field/4,916-5,581 ft) and Sc-2 (carbonate/limestone) has changed and could be correlated to

dissolution of calcite in those samples. Quantitavely, no apparent change could be seen by comparing before and after carbon dioxide treatment. This was explained by the very low amount of dissolution that occurred. It is possible that if the epoxy had been dyed correctly in the second set that the digital method would have caught a slight difference.

4. The examined lithologic units in the Heidelberg field are probably all suitable for enhanced oil recovery. However, formation of gypsum, and resulting porosity loss, in the Eutaw and Smackover Formations could affect long-term production. Each of the lithologies studied would probably be lithologically suitable for long term storage and captured carbon dioxide. However, this study did not consider features such as fractures and regional faults and would make an oil field unsuitable for carbon storage.

REFERENCES

Ahlbrandt, T. S., 1999, Conventional natural gas provinces of the world: AAPG International Conference and Exhibition, p. 2-5.

Benson, D. J., 1988, Depositional history of the Smackover Formation in southwest Alabama: Gulf Coast Association of Geological Societies Transactions, Vol. 38, p. 197-205.

Bennett, L. B., Mancini, E. A., and Markham, T. P., 2000, Salt anticline play in the Mississippi interior salt basin: Gulf Coast Association of Geological Societies Transactions, Vol. 50, p. 261-268.

Buffler, R. T., and Sawyer, D. S., 1985, Distribution of the crust and early history, Gulf of Mexico Basin: Gulf Coast Association of Geological Societies Transactions, Vol. 35, p. 333-344.

Collins, K. M., 2008, Petrography of the Cook-McCormick core, Eutaw Formation, Heidelberg Field Mississippi and relationship to microbial permeability profile modification, M.S. Thesis, Mississippi State University.

Deutsch, W. 1997. Groundwater geochemistry: fundamentals and applications to contamination, p. 80-82.

Emberley, S., Hutcheon, I., Shevalier, M., Durocher, K., Gunter, W. D., and Perkin, E H., 2004, Geochemical monitoring of fluid-rock interaction and CO_2 storage at the Weyburn CO_2-injection enhanced oil recovery site, Saskatchewan, Canada. Energy, Vol. 29, p. 1393-1401.

Emberley, S., Hutcheon, I., Shevalier, M., Durocher, K., Mayer, B., Gunter, W. D., and Perkin, E H., 2005, Monitoring of fluid-rock interaction and CO_2 storage through produced fluid sampling at the Weyburn CO_2-injection enhanced oil recovery site, Saskatchewan, Canada. *Appl. Geochem*., Vol. 20, p. 1131-1157.

Gunter, W. D., Wiwchar, B., and Perkins, E. H., 1997, Aquifer disposal of CO(2)-rich greenhouse gases: Extension of the time scale of experiment for CO(2)-sequestration reaction by geochemical modeling. Mineral. Petrol. Vol. 59, p. 121-140.

Gunter, W. D., Perkins, E. H., and Hutcheon, I., 2000, Aquifer disposal of acid gases: Modeling of water-rock reactions for trapping acid wastes. Appl. Geochem., Vol. 15, p. 1085-1095.

Hughes, D. L., 1968, Salt tectonics as related to several Smackover fields along the northeast rim of the Gulf of Mexico basin: Gulf Coast Asssociation of Geological Societies transactions, Vol. 18, p. 320-330.

Intergovernemental Panel on Climate change (IPCC), 2005, IPCC special report on carbon dioxide capture and storage, prepared by by working Group III of the IPCC (Metz, B., Davidson, O., De Connicik, H. C., Loss, M., and Meyer, L. A., eds.): New York, Cambridge University press, 442 p.

Kaldi, J. G., Gibson-Poole, C. M., and Payenberg, T. H. D., 2009, Geological input to selection and evaluation of carbon dioxide geosequestration sites, in M. Grobe, J. C. Pashin, and R. L. Dodge, eds., Carbon dioxide sequestration in geological media-State of the science: AAPG Studies in Geology 59, p. 5-16.

Kaszuba, J. P., Janecky, D. R., and Snow, M. G., 2003, Carbon dioxide reaction processes in a model brine aquifer at 200°C and 200 bars: Implications for geological sequestration of carbon. *Appl. Geochem.,* Vol. 18, p. 1065-1080.

Kaszuba, J. P., Janecky, D. R., and Snow, M. G., 2005, Experimental evaluation of mixed fluid reactions between supercritical carbon dioxide and NaCl brine: Relevance to the integrity of a geologic carbon repository. *Chem. Geol.,* Vol. 217, p. 277-293.

Kingston, D. R., Dishroon, C. P., and Williams, P. A., 1983, Global basin classification system: American Association of Petroleum Geologists Bulletin, Vol. 71, p. 576.

Klett, T. R., Ahlbrandt, T. S., Schmoker, J. W., Dolton, G. L., 1997, Ranking of the world's oil and gas provinces by known petroleum volumes, Washington, D.C, U.S. Geological Survey.

MacRae, G., and Watkins, J. S., 1996, Desoto Canyon Salt Basin: tectonic evolution and salt structural styles. In structural Framework of the Northern Gulf of Mexico (Ed. By J. O. Jones and R. L. Freed, Special Pubilcation of Gulf Coast Association of Geological Societies), p. 53-61.

Mancini, E. A., Puckett, M. T., William, C. P., Panetta, B. J., 1999, Basin analysis of Mississippi interior salt basin and petroleum system modeling of the Jurassic Smackover Formation, Eastern Gulf Coastal Plain, Tuscaloosa, the University of Alabama.

Mancini, E. A., Parcell, W. C., Puckett, T. M., and Llinos, J. C., 2001, Topical report 4 – Basin and petroleum migration modeling of the Mississippi Interior Salt Basin: US Department of Energy report, p. 46 and appendixes.

Mancini, E.A., 1994, Paleoenviroments of the Tombigbee Sand member of the Eutaw Formation (Upper Cretaceous) of eastern Mississippi and western Alabama. American Association Petroleum Geologists Bulletin, Vol. 78, p. 1468.

Marini, L. 2007, Geological Sequestration of Carbon Dioxide Thermodynamics, Kinetics, and Reaction Path Modeling. Amsterdam: Elsevier.

Martin, R. G., 1978, Northern and eastern Gulf of Mexico continental margin: Stratigraphy and structural framework: American Association of Petroleum Geologists Bulletin studies in Geology, Vol. 7, p. 21-42.

McCullough, R. A., 1944, Geology of the Heidelberg oil field. Oil, Vol. 4, p.8-9.

Miller, J. A., 1982, Structural control of Jurassic sedimentation in Alabama and Florida: AAPG Bulletin, Vol. 66, p. 1289-1301.

Mississippi Geological Society, 1957, Heidelberg field, Jasper County, Mississippi: In Mesozoic-Paleozoic producing areas of Mississippi and Alabama. p. 62-63.

Montgomery, S. L., and Ericksen, R. L., 1997, Dry creek salt dome, Mississippi Interior Salt Basin: American Association of Petroleum Geologists Bulettin, Vol. 81, p. 351-366.

Morse, W. C., 1944, The Heidelberg oil field, Oil, Vol. 4, p. 392.

Nesse, D. W. 2000. Introduction to Mineralogy. New York, New York: Oxford University Press, Inc. p. 341-344.

Oxley, M.L., and Herlihy, Daniel E., 1974, The Bryan field; a sedimentary anticline, Gulf Coast Association of Geological Societies Transactions, Vol. 24, p. 42-48.

Pearce, J. M., Holloway, S., Wacker, H., Nelis, M. K., Rochelle, C., and Bateman, K., 1996, Natural occurrences as analogues for the geological disposal of carbon dioxide. Energy Convers. Manage., Vol. 37, p. 1123-1128.

Pellant, C. 2002. Rocks and Minerals. New York, New York: Dorling Kindersley, Inc., p. 341-344.

Pilger Jr, R. H., 1981, The opening of the Gulf of Mexico: Implications for the tectonic evolution of the northern Gulf Coast, Gulf Coast Association of Geological Societies Transaction, Vol. 31, p. 377-381.

Pirlet, H., Wehrmann, L. M., Brunner, B., Franks, N., Dewanckele, J., Van Rooij, D., Foubert, A., Swennen, R., Naudts, L., Boone, M., Cnudde, V., and Henriet, J-P., 2010, Diagenetic formation of gypsum and dolomite in a cold-water coral mound in the Porcupine seabight, off Ireland. Sedimentology, The Journal of the International Association of Sedimentology., Vol. 57, p. 786-805.

Rackley, S. A. 2010. Carbon capture and storage. Burlington: Butterworth-Heinemann.

Rochelle, C., Bateman, K., and Pearce, J. M., 1996, Fluid-rock interactions resulting from the underground disposal of carbon dioxide. In: Bottrell, S.H (ed.), *Proc. 4th Int. Symp. Geochem. Earth's Surf.*, University of Leeds, Dept. of Earth Sciences, Leeds, p. 448-452.

Salvador, A., 1987, Late Triassic-Jurassic paleogeography and origin of the Gulf of Mexico Basin: AAPG Bulettin, Vol. 71, p. 419-451.

Salvador, A., 1991, Origin and development of the Gulf of Mexico Basin, *in* A. Salvador, ed, The Gulf of Mexico Basin: Geological Society of America, Decade of North American Geology, Vol. J, p. 389-444.

Sass, B. M., Gupta, N., Ickes, J. A., Engelhard, M. H., Baer, D. R., Bergman, P., and Byrer, C., 2001, Interaction of rock minerals with carbon dioxide and brine: A hydrothermal investigation. 1 st National Conference on Carbon Sequestration. National Energy Technology Laboratory, Washington DC, http://www.netl.doe.gov.

Songgiao, Luo., 1993, Subsurface structure and hydrocarbon occurrence, cretaceous rocks of Maxie and Pistol Ridge fields, Southeastern Mississippi. M.S Thesis, University of Southern Mississippi.

Sohl, N. F., Martinez R., E., Salmerón-Ureña, P., and Soto-Jaramillo, F., 1991, Upper Cretaceous, in Salvador, A., ed., The Gulf Coast of Mexico Basin: Boulder, Colorado, Geological Society of America, The Geology of North America, v. J.

Van Siclen, D. C., 1984, Early opening of initially-closed Gulf of Mexico and central North Atlantic Ocean: Transactions of the Gulf Coast Association of Geological Socities, Vol. 34, p. 265-275.

White, J. V., Kirkland, B. L., and Gournay, J. P., 1998, Quantitative determination of thin sections using digitized image, J. Sediment. Petrol., Vol. 68, No 1, p. 221-222.

White, S.P., Allis, R.G., Moore, J., Chidsey, T., Morgan, C., Gwynn, W., and Adams, M., 2005, Simulation of reactive transport of injected CO_2 on the Colorado Plateau, Utah, USA. Chem. Geol., Vol. 217, p. 387-405.

Winker, C. D., and Buffler, R. T., 1988, Paleogeographic evolution of early deep-water Gulf of Mexico and margins, Jurassic to middle Cretaceous: AAPG Bulletin, Vol. 72, p. 318-346.

Wood, M. L., and Walper, J. L., 1974, The evolution of the interior Mesozoic basin and the Gulf of Mexico: Gulf Coast Association of Geological Societies Transactions, Vol. 24, p. 31-41.

Xu, T., Apps, J. A., and Pruess, K., 2000, Analysis of mineral trapping for CO_2 disposal in deep aquifers. Lawrence Berkley National Laboratory Report LBLN-47315, Berkley, CA.

Xu, T., Apps, J. A., and Pruess, K., 2004, Numerical simulation of CO_2 disposal by mineral trapping in deep aquifer. *Appl. Geochem.* , Vol. 19, p. 917-936.